The Ohio State University

AMPLITUDE AND ANGLE OF ARRIVAL MEASUREMENTS ON A 28.56 GHz EARTH-SPACE PATH

D.M.J. Devasirvatham and D.B. Hodge

The Ohio State University

ElectroScience Laboratory

Department of Electrical Engineering
Columbus, Ohio 43212

Technical Report 712759-4
Contract No. NASW-3393
March 1981

National Aeronautics and Space Administration Headquarters
Washington, D.C. 20546

NOTICES

When Government drawings, specifications, or other data are used for any purpose other than in connection with a definitely related Government procurement operation, the United States Government thereby incurs no responsibility nor any obligation whatsoever, and the fact that the Government may have formulated, furnished, or in any way supplied the said drawings, specifications, or other data, is not to be regarded by implication or otherwise as in any manner licensing the holder or any other person or corporation, or conveying any rights or permission to manufacture, use, or sell any patented invention that may in any way be related thereto.

SECURITY CLASSIFICATION OF THIS PAGE *(When Data Entered)*

REPORT DOCUMENTATION PAGE		READ INSTRUCTIONS BEFORE COMPLETING FORM
1. REPORT NUMBER	2. GOVT ACCESSION NO.	3. RECIPIENT'S CATALOG NUMBER
4. TITLE *(and Subtitle)* AMPLITUDE AND ANGLE OF ARRIVAL MEASUREMENTS ON A 28.56 GHz EARTH-SPACE PATH		5. TYPE OF REPORT & PERIOD COVERED Technical Report 6. PERFORMING ORG. REPORT NUMBER ESL 712759-4
7. AUTHOR(s) D.M.J. Devasirvatham and D.B. Hodge		8. CONTRACT OR GRANT NUMBER(s) NASW-3393
9. PERFORMING ORGANIZATION NAME AND ADDRESS The Ohio State University ElectroScience Laboratory, Department of Electrical Engineering Columbus, Ohio 43212		10. PROGRAM ELEMENT, PROJECT, TASK AREA & WORK UNIT NUMBERS
11. CONTROLLING OFFICE NAME AND ADDRESS NASA Headquarters HQ Contracts and Grants Division Washington, D.C. 20546		12. REPORT DATE March 1981 13. NUMBER OF PAGES 45
14. MONITORING AGENCY NAME & ADDRESS*(if different from Controlling Office)*		15. SECURITY CLASS. *(of this report)* Unclassified 15a. DECLASSIFICATION/DOWNGRADING SCHEDULE

16. DISTRIBUTION STATEMENT *(of this Report)*

17. DISTRIBUTION STATEMENT *(of the abstract entered in Block 20, if different from Report)*

18. SUPPLEMENTARY NOTES

19. KEY WORDS *(Continue on reverse side if necessary and identify by block number)*

Angle of Arrival	Microwave
Attenuation	Propagation
COMSTAR Satellite	Rain
Earth-Space Paths	Self-Phased Array
Millimeter Wave	Scintillation

20. ABSTRACT *(Continue on reverse side if necessary and identify by block number)*

This report describes amplitude and angle of arrival measurements on an earth-space path, using the 28.56 GHz COMSTAR D_3 satellite beacon. These measurements were made by The Ohio State University ElectroScience Laboratory during the period September 1978 to September 1979. Monthly, quarterly, and annual distributions of attenuation, angle of arrival, and variance of both these parameters are reported.

During this period, fades exceeding 29 dB for .001% of the time and angle of

DD FORM 1 JAN 73 1473 EDITION OF 1 NOV 65 IS OBSOLETE

Unclassified
SECURITY CLASSIFICATION OF THIS PAGE *(When Data Entered)*

arrival fluctuations exceeding 0.12 degrees for .01% of the time were observed. The experiment is described, samples of data are presented and the data analysis is summarized.

CONTENTS

LIST OF FIGURES

LIST OF FIGURES, CONT.

LIST OF TABLES

INTRODUCTION

A number of propagation effects influence communication signals at frequencies above 10 GHz. The most widely studied of these is the attenuation caused by rain and the atmospheric gases. In addition, atmospheric turbulence in the troposphere has two primary effects. One is the perturbation of the amplitude of the received signal by scattering. The other is the distortion of the wave front or physical bending of the ray path, changing its apparent angle of arrival. The degree of these effects changes from moment to moment and is influenced directly by the weather.

This report documents the ongoing angle of arrival and attenuation measurements conducted at The Ohio State University with the 28.56 GHz beacon signals from the COMSTAR D_1, D_2 and D_3 geosynchronous satellites. This experiment is an extension of an earlier experiment, which provided statistics of the angle of arrival of an 11.7 GHz signal from the CTS satellite. The CTS experiment and results are described in References [1,2,3].

Measurements in both the CTS and COMSTAR experiments were made with a co-planar self-phased array having elements located at the corners of a square. The element outputs are coherently summed to measure the array sum amplitude. The electrical phase differences between the outputs of the elements are a measure of the angle of arrival of an equivalent plane wave front. The decorrelation between the differential phases is a measure of the distortion of the actual wave front reaching the antennas.

The progress of the experiment is traced briefly. The equipment used is documented. Sample data are shown and the results of the data analysis are presented.

EQUIPMENT

Transmitter

The space craft transmitter had an effective radiated power of 51dBm. It was designed for very high frequency and phase stability. However, these specifications were degraded after few months of use

when problems developed in the power supply subsystem. This was serious enough to necessitate extensive modifications of the receivers used for this experiment.

Receivers

The receiving equipment (Figures 1 and 2) consists of a co-planar, four-element, self-phased array, receivers and the monitoring and data logging system. The equipment was used earlier together with the Communications Technology Satellite (CTS) to perform similar measurements at 11.7 GHz and has been documented elsewhere [1]. The antenna feeds and receiver front-ends were subsequently modified for operation at 28.56 GHz. Extensive work was done on the front-end (rf) section, the tracking loops and detectors to accommodate the characteristics of the spacecraft beacon as well as the new frequency. The following brief description will emphasize these important differences.

The parameters of the four-element co-planar array (Figure 1) are given in Table 1. The elements are large enough to provide reasonable gain while having a beamwidth of 1.2^{o}. This ensures nearly constant gain and phase characteristics for all positions of the satellite during its diurnal motion, eliminating the need for mechanical steering. The 1 meter inter-element spacing gives high sensitivity to changes in angle of arrival.

The radio frequency front-ends use low noise semiconductor down-convertors with a noise figure of 4 dB. The intermediate frequency signals at 30 MHz, 3.0 MHz and 455 kHz are corrected for phase differences using phase locked "Inner Loops" referenced to a common, highly stable 455 kHz oscillator. The error voltages produced by the reference phase detectors control nominal 2.545 MHz variable frequency crystal oscillators (VCXO). The shifts in phase required of these VCXO's to keep the incoming signals in phase alignment are measured using differential phase detectors, thus measuring the phase differences between the signals. These differential phase detectors have an unambiguous range of $\pm\ 360^{o}$ (nominal). Furthermore, beyond this range, they make a

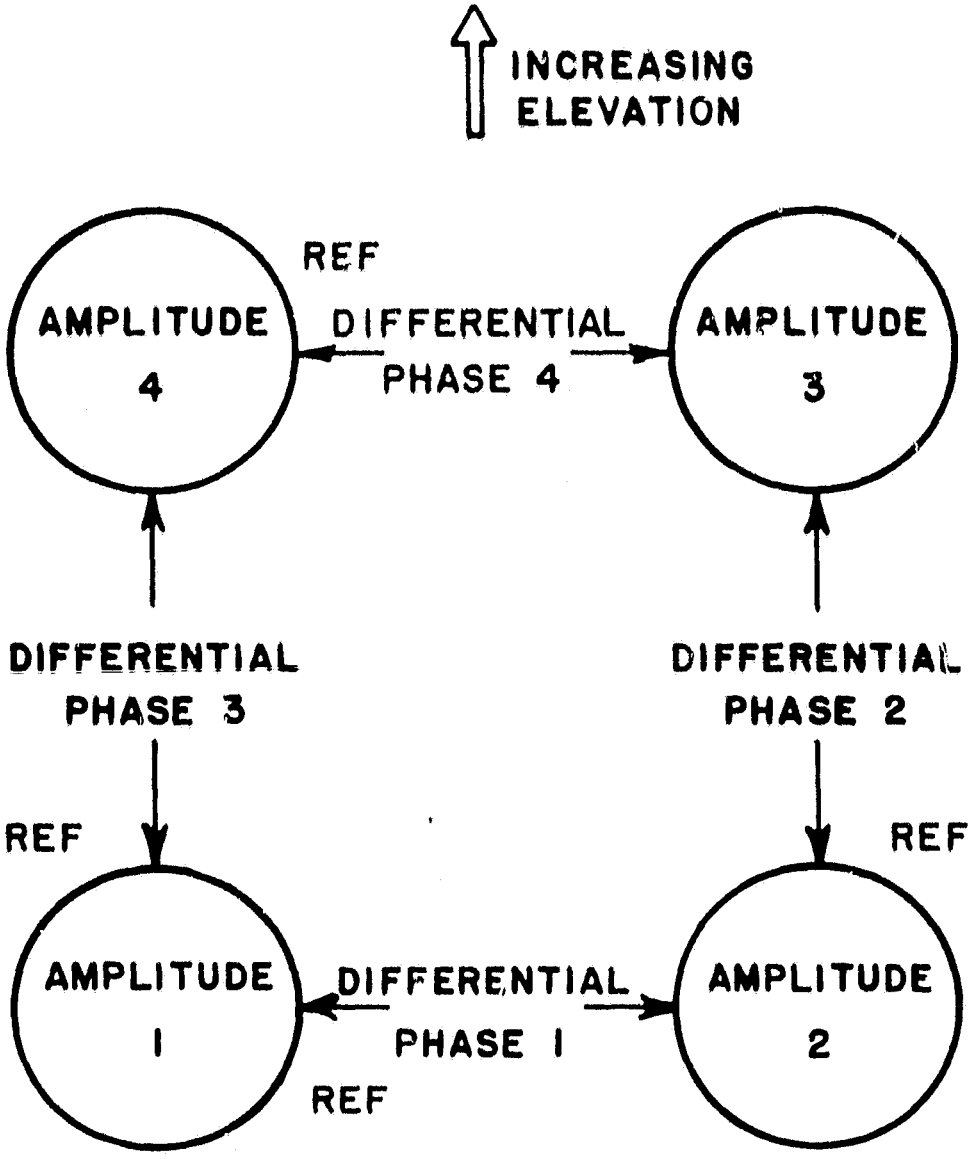

Figure 1. Self-phased array configuration.

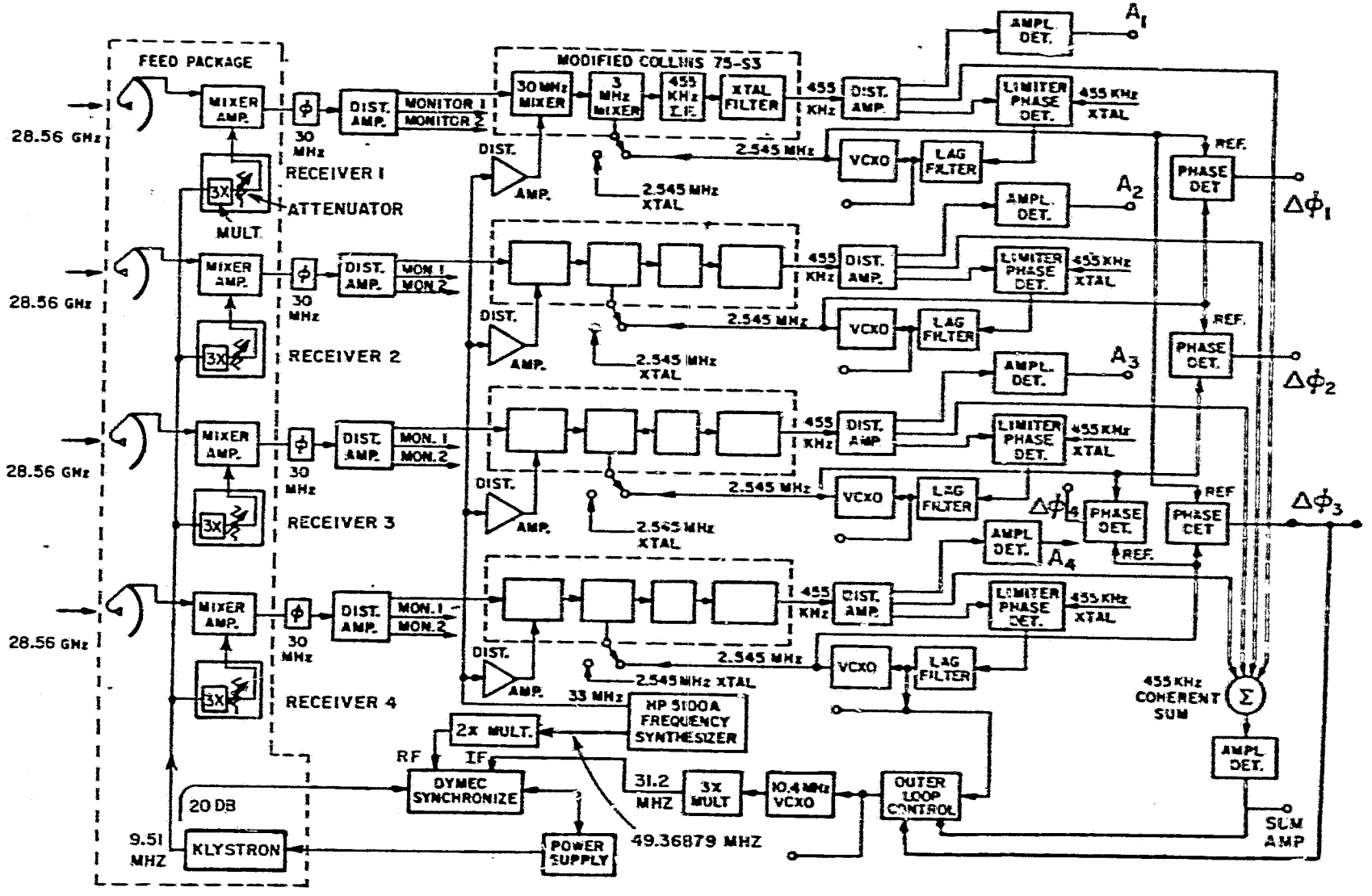

Figure 2. Self phased array receiver expanded block diagram.

TABLE I - RECEIVING ARRAY PARAMETERS

Frequency	28.56 GHz
No. of Elements	4 - Coplanar
Type	Focal Point Feed Parabolic
Element Diameter	0.6m (57λ)
Beamwidth	1.2^{o}
Inter-element Spacing	1.0m (95.4λ)
Polarization	Linear

sharp transition and resume their linear characteristics. By counting the number of transitions and appropriately adding or subtracting multiples of 360^{0}, this range can be extended indefinitely.

The receiver bandwidth was initially 80 Hz and was later increased to 165 Hz when the stability of the spacecraft beacon lessened. However, the diurnal motion of the satellite produces Doppler frequency shifts in the incoming signal of nearly 20 kHz. Hence, an "Outer Loop", controlled by one of the reference phase detectors, shifts the frequency of the common Klystron first local oscillator to keep the signal within the passband of the receivers. Since this corrects all four channels identically, it does not affect the phase differences between the channels. The outer loop control, which was also extensively re-designed following the earlier CTS experiment, has a response which is much slower than the signal scintillation and thus responds only in an average sense to minimize its effect on the parameters being measured. In case of signal loss, as in heavy rain, the outer loop controller is provided with a two speed sweep circuit to permit re-acquisition after a delay. Signal amplitude is also monitored to aid in this task.

The four individual signal amplitudes as well as the coherent sum signal are detected by square law detectors. The amplitude outputs range from 0 to +5V, while the differential phase detectors provide outputs in the -5 to +5 volt range.

DATA RECORDING

The outputs are digitized at 1/3 Hz (slow rate) at all times and at 10 Hz when desired (fast rate) after filtering to avoid aliasing. The resolution is 8 bits. Data were acquired 24 hours a day under the control of an Hewlett Packard 2116B minicomputer and recorded on 7-track magnetic tape. During the course of this experiment, the 7-track tape unit was replaced by a 9-track tape unit for more convenient data analysis on the laboratory computer system. For details of the data acquisition system refer to Reference [2].

The 1/3 Hz sampling rate, though precluding spectral analysis of the data, is fast enough to provide statistical measurements, such as the mean and variance of the relatively slow atmospheric phenomena, while keeping the massive amount of data obtained within reasonable bounds.

The length of a slow sample rate record was 32 samples, representing 96 seconds in time. Each sample recorded nine channels; namely, the four receiver amplitudes, the coherent sum amplitude and the four differential phase values. Each record header also contains various station keeping parameters such as time and status of sense switches. Data recording was automatically idled if monitoring circuits determined that the receiving system had lost phase lock. Upon automatically reacquiring lock, normal data acquisition resumed.

CALIBRATION

Amplitude Calibration

The amplitude calibration scheme is shown in Figure 3 for a single channel. The output of a local signal generator is fed into the 30 MHz intermediate frequency chain through a power combiner so that front-end noise is included. The signal generator level is adjusted to give 5 volts at the receiver output terminal. This is taken as the 0 dB reference level. The generator output is then progressively reduced by a calibrated attenuator, giving the received signal level as a function of the receiver output voltage, V_{out}.

Differential Phase Calibration

The differential phase detectors have an extremely wide range of almost $\pm 360^{0}$. Since no phase shifter capable of shifting the phase of one of the input signals with respect to the others through that range was available, an indirect scheme was adopted as shown in Figure 4.

The nominal frequency of the inputs is 2.545 MHz. Two stable signal generators were used. One was set to 2.545 MHz and the other offset to $2.545 \pm \varepsilon$ MHz, where ε was a very small fraction of one Hz. The differential phase detector output was recorded on a strip chart.

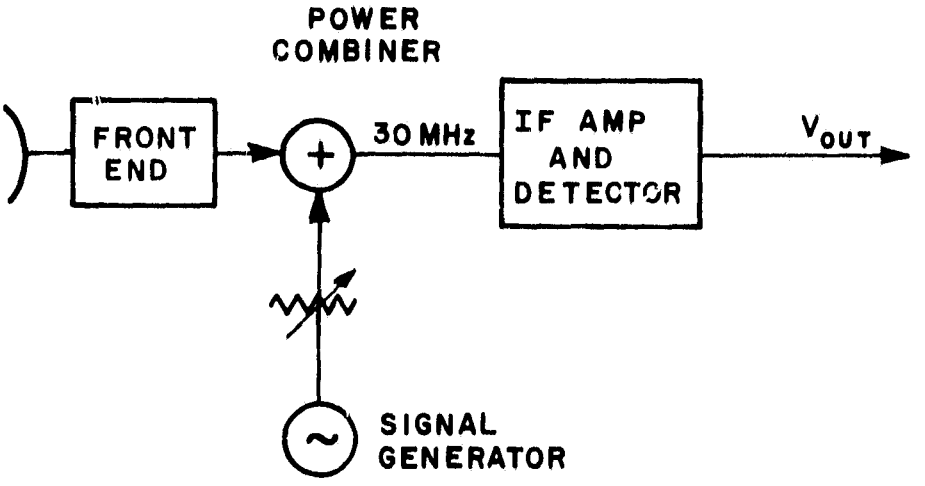

Figure 3. Amplitude Calibration Scheme.

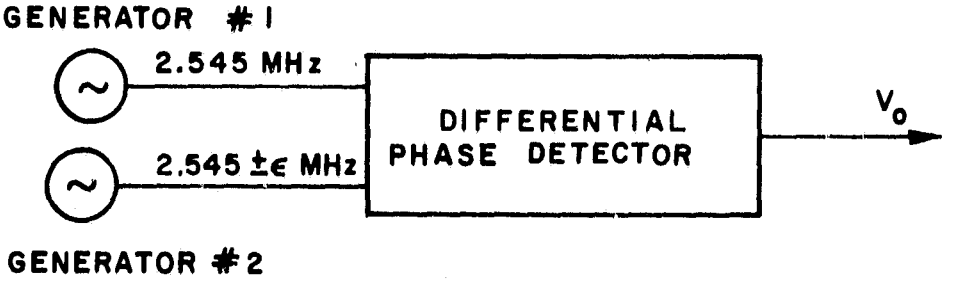

Figure 4. Differential phase calibration scheme.

Thus, as the signals swept past each other, the phase difference changed through -360^{0} to $+360^{0}$. The output was found to be extremely linear.

HISTORY OF THE EXPERIMENT

The COMSTAR D_1 and D_2 spacecraft were placed in geosynchronous orbits at approximately 128^{0}W and 95^{0}W longitude, respectively, and were scheduled to be turned off in September, 1978. The D_3 satellite was launched in June, 1977 and positioned at 87^{0}W longitude. We hoped to acquire first D_2 and then D_1 in July, 1978, and finally switch to D_3 in September, 1978, for long term measurements.

However, problems with the ground equipment did not permit full data acquisition to commence until September, 1978. Thus, very limited data were collected utilizing D_1 and D_2 in August, 1978.

Excellent data were collected using the D_3 satellite until mid-December, 1978, when instabilities developed suddenly in the beacon frequency. Discrete frequency jumps exceeding 50 Hz were observed, making tracking virtually impossible with the existing 80 Hz receiver bandwidth. While some switching in the spacecraft improved the situation somewhat, conditions deteriorated again.

As a result, the receiver data bandwidth was widened to 165 Hz and the outer loop control was modified extensively. These steps permitted data acquisition to resume. Subsequent action by spacecraft controllers calmed the frequency and phase jitters somewhat; but the signals never regained the initial purity. Due to the wider bandwidth, the system margin dropped to about 28 dB. Link margin calculations are presented in Table 2.

It was also discovered in April, 1979, that differential phase #4 was not being recorded due to equipment malfunction. After this was corrected, complete data acquisition was resumed in May, 1979, and has continued since.

The data periods covered in this report are given in Table 3.

TABLE II - D_3 LINK CALCULATIONS (FOR A SINGLE CHANNEL)

	Frequency 28.56 GHz	Linear Polarization	
	ERP	+ 51	dBm
	Free Space Loss	-212.6	dB
	Clear Air Loss (H_2O, O_2)	- 1.1	dB
	Receiver Antenna Gain (0.6m)	+ 42.7	dB
	Received Power	-120	dBm
	Receiver Noise		
(a)	Bandwidth 80Hz	-151	dBm
	Signal/Noise Ratio	31	dB
(b)	Bandwidth = 165 Hz	-148	dBm
	Signal/Noise Ratio	28	dB

TABLE III - USABLE DATA PERIODS

Month	Hours of Data
D_1 and D_2 operations	
July, 1978	186[1]
August	212[2]
D_3 operations	
September	398
October	385
November	557
December	456
January, 1979	479
February	568
March	581
April	570
May	585
June	524
July	536
August	668
September	419
TOTAL	6726

[1]System debugging.

[2]Lightning transient in data system.

EDITING AND ANALYSIS

Editing

The approximately 6726 hours of data were edited using the laboratory interactive computer CRT display. This resulted in a control file for each reel of tape, which was then used to control the analysis programs. The analysis programs also contained checks and safeguards to reject unsuitable data which may not have been detected in the editing process. The following criteria were applied:

(a) Based on experiment logs and visual inspection, the quality of the data was considered acceptable.

(b) Only records containing the full 32 samples were selected.

(c) If any channel was not phase locked, the entire record was discarded. This was done to ensure the same data base for all the channels.

Analysis

Let the difference in electrical phase between the outputs of two elements be $\Delta\phi$ (Figure 5).

The conversion from differential phase, $\Delta\phi$, to the apparent angle of arrival, α, of the incident beam, assuming a planar wave front is made as follows:

$$\Delta\phi = kD\sin\alpha \qquad , \alpha = \sin^{-1}\left(\frac{\Delta\phi}{kD}\right)$$

where $k = \frac{2\pi}{\lambda}$ = the propagation constant of the wave

D = separation between the elements

For D = 1 meter, a frequency of 28.56 GHz, and small deviations in α

$$\frac{\Delta\phi}{\alpha} = 597 \qquad \text{(electrical degree/spatial degree).}$$

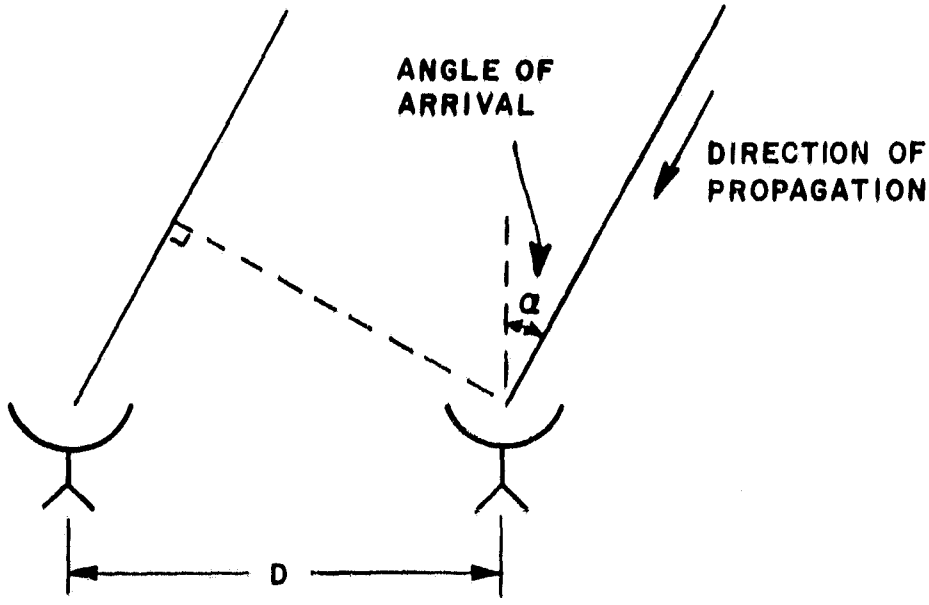

Figure 5. Apparent angle of arrival.

It must be emphasized that α is an apparent angle of arrival, i.e., that which would be observed if the received signal were an ideal plane wave. It is recognized that, in general, the phase front of the incoming wave may be distorted and, thus, would be a summation of plane waves.

Let v_i be the ith sample in a record of the output voltage of a receiver. $\Delta\phi_i$ is the corresponding differential phase value. Then for N samples:

(a) Mean signal level

$$\overline{V} = \frac{1}{N} \sum_{i=1}^{N} v_i \qquad \text{(volts)}$$

(b) Signal variance

$$\sigma^2_V = \frac{1}{N} \left\{ \sum_{i=1}^{N} \frac{(v_i - \overline{V})^2}{\overline{V}^2} \right\} \qquad \text{(numeric)}$$

$$\sigma^2_{V(dB)} = 10 \log_{10} \frac{1}{N} \left\{ \sum_{i=1}^{N} \frac{(v_i - \overline{V})^2}{\overline{V}^2} \right\} \qquad \text{(dB)}$$

(c) Mean differential phase

$$\overline{\Delta\phi} = \frac{1}{N} \sum_{i=1}^{N} \Delta\phi_i \qquad \text{(degrees)}$$

(d) Differential Phase variance

$$\sigma^2_{\Delta\phi(dB)} = 10 \log_{10} \frac{1}{N} \left\{ \sum_{i=1}^{N} \frac{(\Delta\phi_i - \overline{\Delta\phi})^2}{\Delta\phi_o{}^2} \right\} \qquad \text{(dB)}$$

where $\Delta\phi_o$ is a reference value chosen to be 1 electrical degree for convenience

(e) Amplitude correlation coefficient

$$\rho_V(\ell,m) = \frac{1}{N}\sum_{i=1}^{N} \frac{(v_i(\ell) - \overline{v}(\ell))(v_i(m) - \overline{v}(m))}{\sigma_V(\ell)\sigma_V(m)}$$

(f) Phase correlation coefficient

$$\rho_{\Delta\phi}(\ell,m) = \frac{1}{N}\sum_{i=1}^{N} \frac{(\Delta\phi_i(\ell) - \Delta\overline{\phi}(\ell))(\Delta\phi_i(m) - \Delta\overline{\phi}(m))}{\sigma_{\Delta\phi}(\ell)\sigma_{\Delta\phi}(m)}$$

where ℓ,m denote the channels between which the correlation is computed.

Note that N = 32 in all cases, since only complete data records were accepted for analysis. Therefore, the statistics computed are for 96 second data intervals.

Since all signals had been calibrated relative to a fixed output level of 5 volts, a running estimate had to made of the actual signal level under clear air conditions in order to measure the depth of fading during fade events. This was achieved by a projection algorithm as follows.

Estimates were based on the maximum instantaneous value of the signal over selected uninterrupted time intervals.

(1) The maximum signal level in the first record in each channel was taken as a starting point

(2) As more records were processed, this maximum was updated by the maximum level over all the records processed. All points were analysed with respect to this point.

Once 13 records (≈20 minutes) were processed, a new maximum value was started and a two point linear fit between this and the previous set maximum was used as the maximum signal level at any point.

After an additional 13 records had been processed a third maximum point was obtained over the next set of records. A 3 point polynomial

fit was now used to estimate the maximum signal level at any instant. Thereafter, if processing continued uninterrupted in time for another 40 records (≈ 1 hour), the first maximum point was discarded and the three point projection was now based on the latest set of maxima.

In this manner, after the rapid initial estimates, sufficient inertia was built into the projection of the maximum level to allow a good estimate of fade depths.

Any break in the valid data of more than 7 minutes, due to idling of data acquisition or unlocking of the receiver, reset the projection and the procedure started again. However, the permissible gap was extended to 15 minutes if it occurred during a fade event. Continuing the projection beyond that was considered to be unreliable.

The different phase projection scheme is identical in concept except that mean values were used instead of maxima. Further, since the mean value of the differential phase changed much more rapidly due to satellite motion, projection times were reduced to 1½ minutes (2 records) per mean estimate initially and after the first 3 points, to about 10 minutes. This was, however, considered slow enough to detect any cases of "phase pulling"; that is, a rapid short term change in mean angle of arrival due to bulk atmosphere effects.

The programs developed for analysis generated amplitude, amplitude variance, angle of arrival and angle of arrival variance distributions. Logs of events, such as fades, unusually large amplitude or angle of arrival scintillations or cases of phase pulling, were produced. Time logs of the periods of data analysed were printed. Distributions of the correlation between channel amplitudes as well as differential phase pairs were obtained during representative data periods.

These statistics were generated on a monthly, quarterly, and annual basis and are presented below.

DATA

Some examples of the received sum signal and three differential phases are shown in Figures 6 through 16. All are Max-min plots showing the trace of the maximum and minimum envelope. $\Delta\phi_2$ and $\Delta\phi_3$ are vertical components while $\Delta\phi_1$ is a horizontal differential phase (see Figure 2). All times are Greenwich Mean Time.

Examples of strong amplitude scintillation without change in signal level in Figures 6 and 7 correlate well with cumulus clouds passing directly through the beam.

Rain's most predictable effect is amplitude fading. Its effect on phase is less apparent. Some deep fades produce very little angle fluctuation, while enhanced angle fluctuation is seen in some very moderate fades.

The 24 hour plot commencing on day 350/1978 at 1800Z, Figure 8, is a typical example of clear weather data following a minor rain fade. The matched change in the elevation angle of the satellite due to its diurnal motion is reflected in $\Delta\phi_2$ and $\Delta\phi_3$ which are a vertical pair of differential phases.

The data on day 6/79 1700Z hours, Figure 9, is of considerable interest. The fairly rapid change in mean angle is unusual, but was observed on a few other occasions. It is known that no satellite repositioning was in progress. A heavy fog was present on this particular midwinter day and was burning off at this time. The vertical physical angle changes by nearly 0.3° within about half an hour. The most likely explanation is that of a duct or layer in the atmosphere, which was subsequently dissipated by the sun. Such a duct or layer might cause bulk refraction and thus lead to this result.

The significance of system noise on the data during deep fades is important as it may contaminate the phase information. The data in Figure 16 is of interest in this regard. It is seen that a 24dB fade at about 1900Z hours on day 240/79 shows greater angle fluctuation than a 27dB fade at 2030 hours, showing that the effects of receiver noise

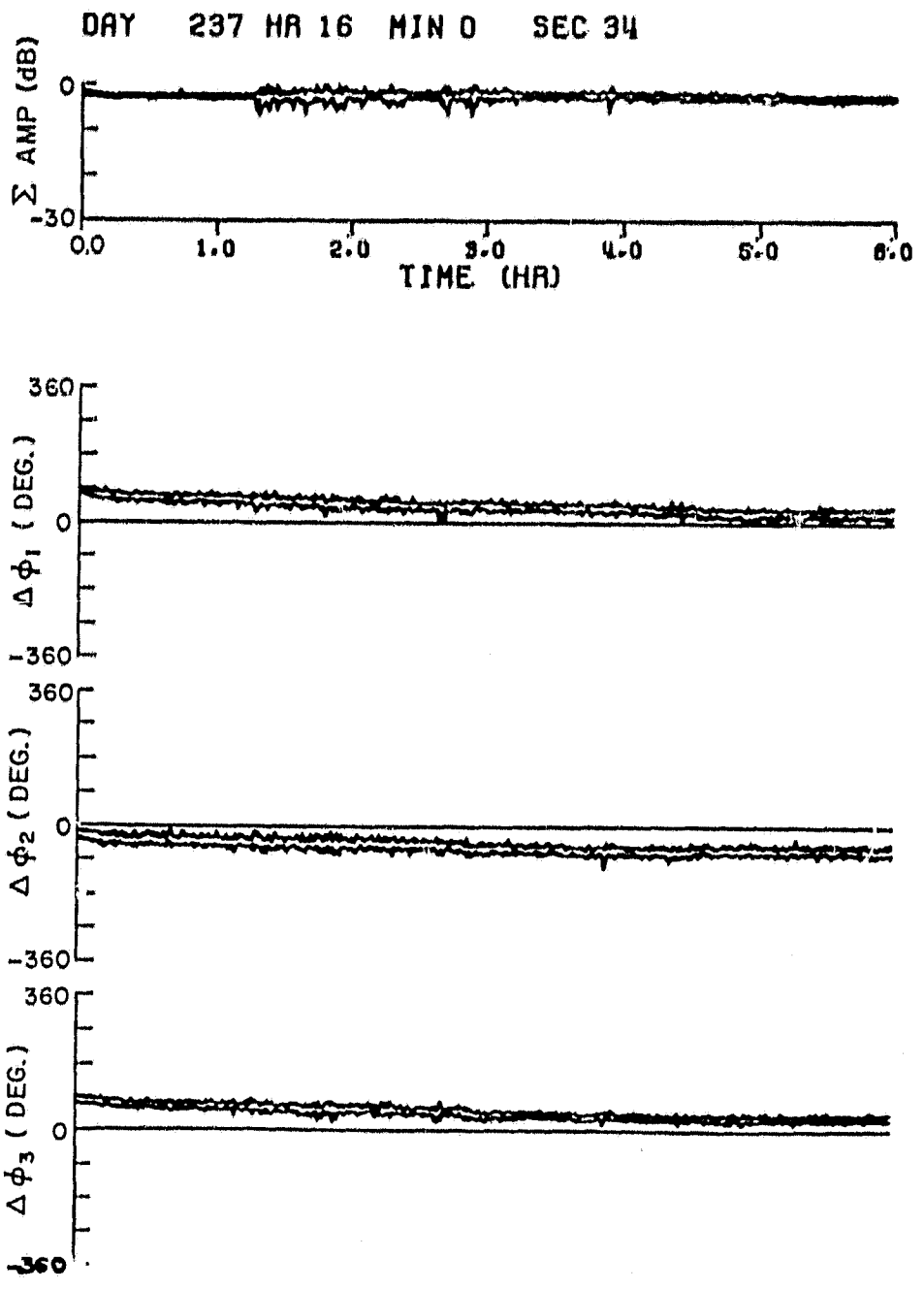

Figure 6. Received Signals on day 237/1978 1600Z
(The number on top is the digital data Tape I.D. Number.)

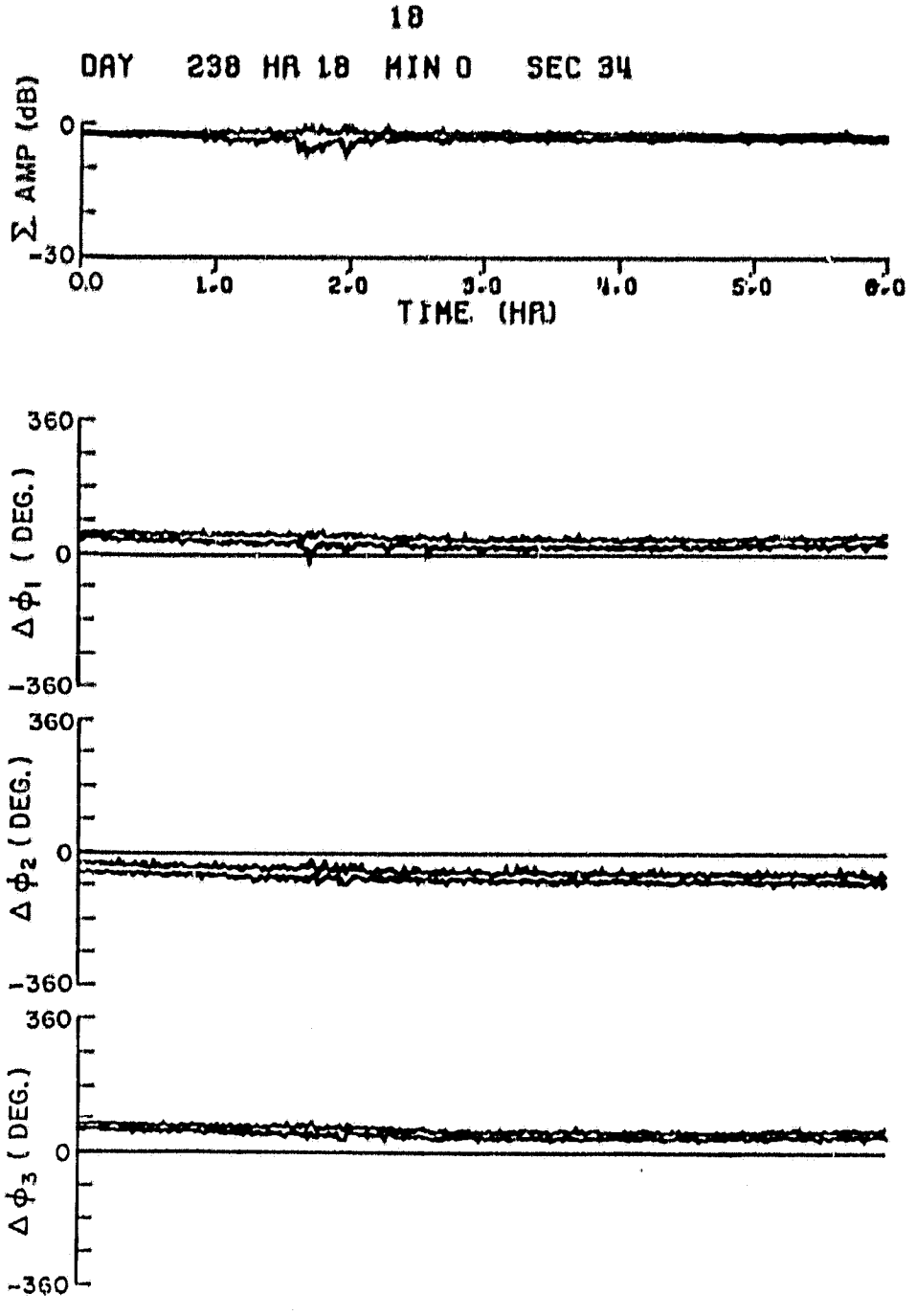

Figure 7. Received signals on day 238/1978. 1800Z

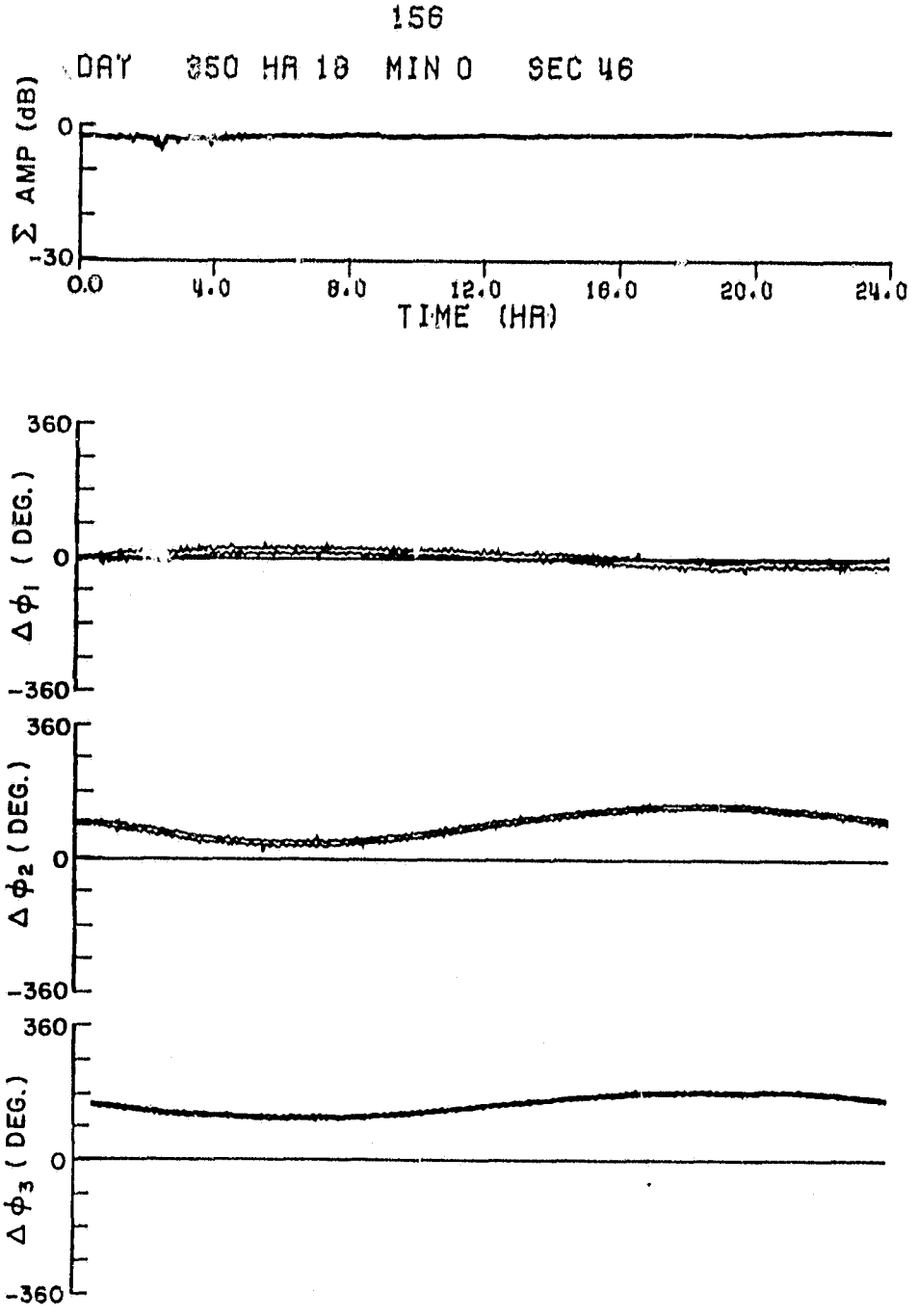

Figure 8. Received signals on day 350/1978. 1800Z

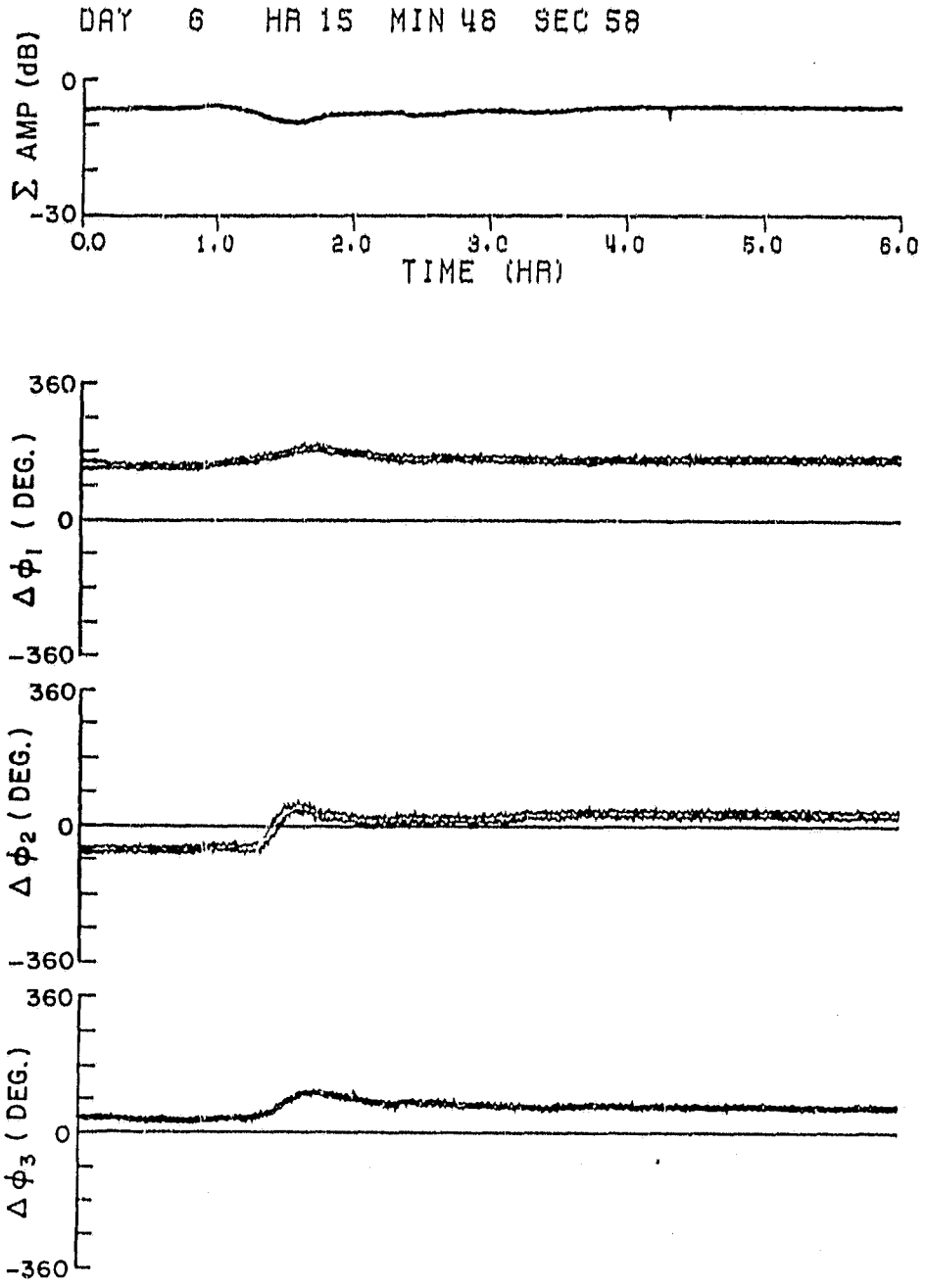

Figure 9. Received signals on day 6/1979 1548Z

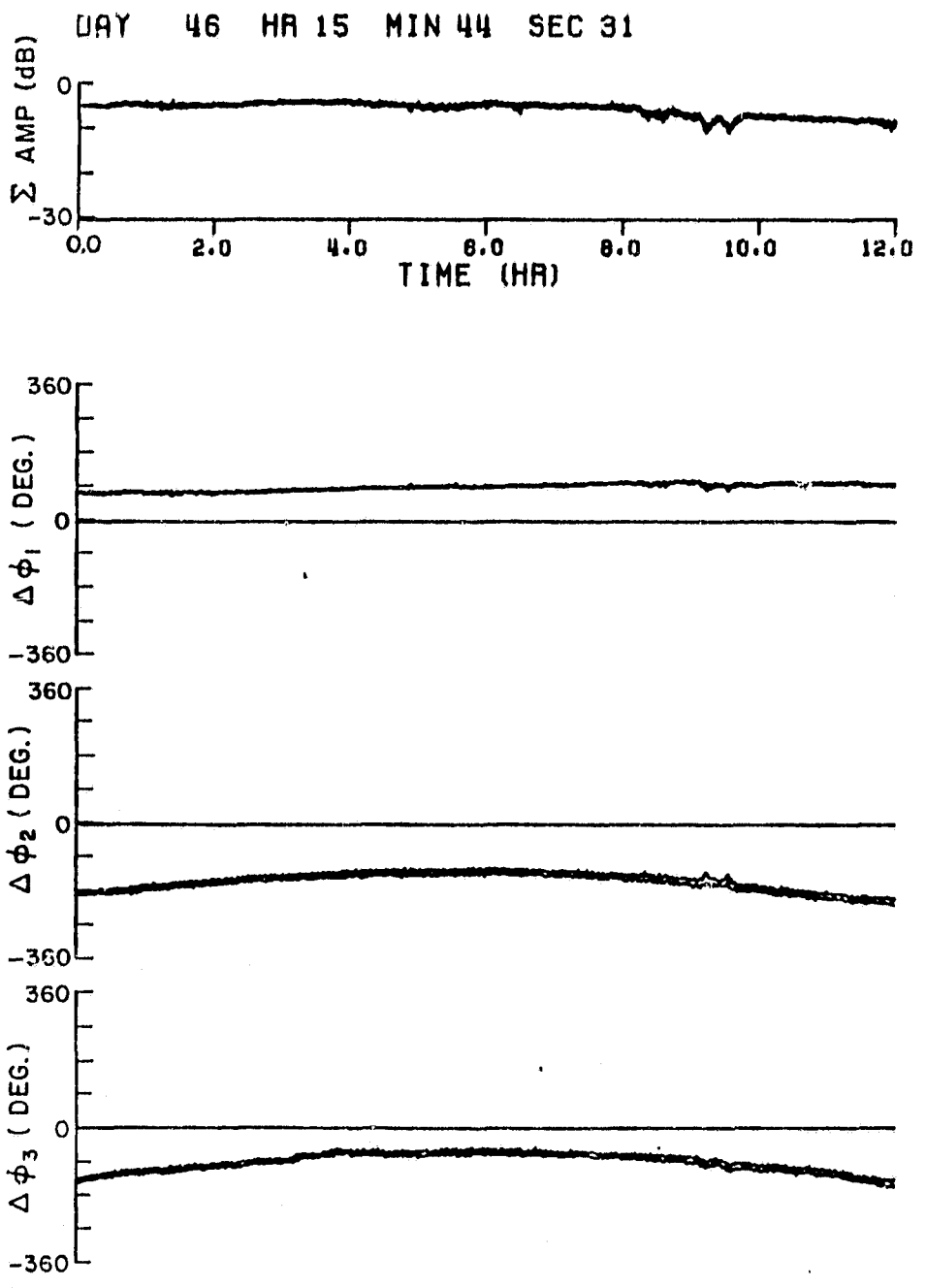

Figure 10. Recieved signals on day 46/1979. 15467

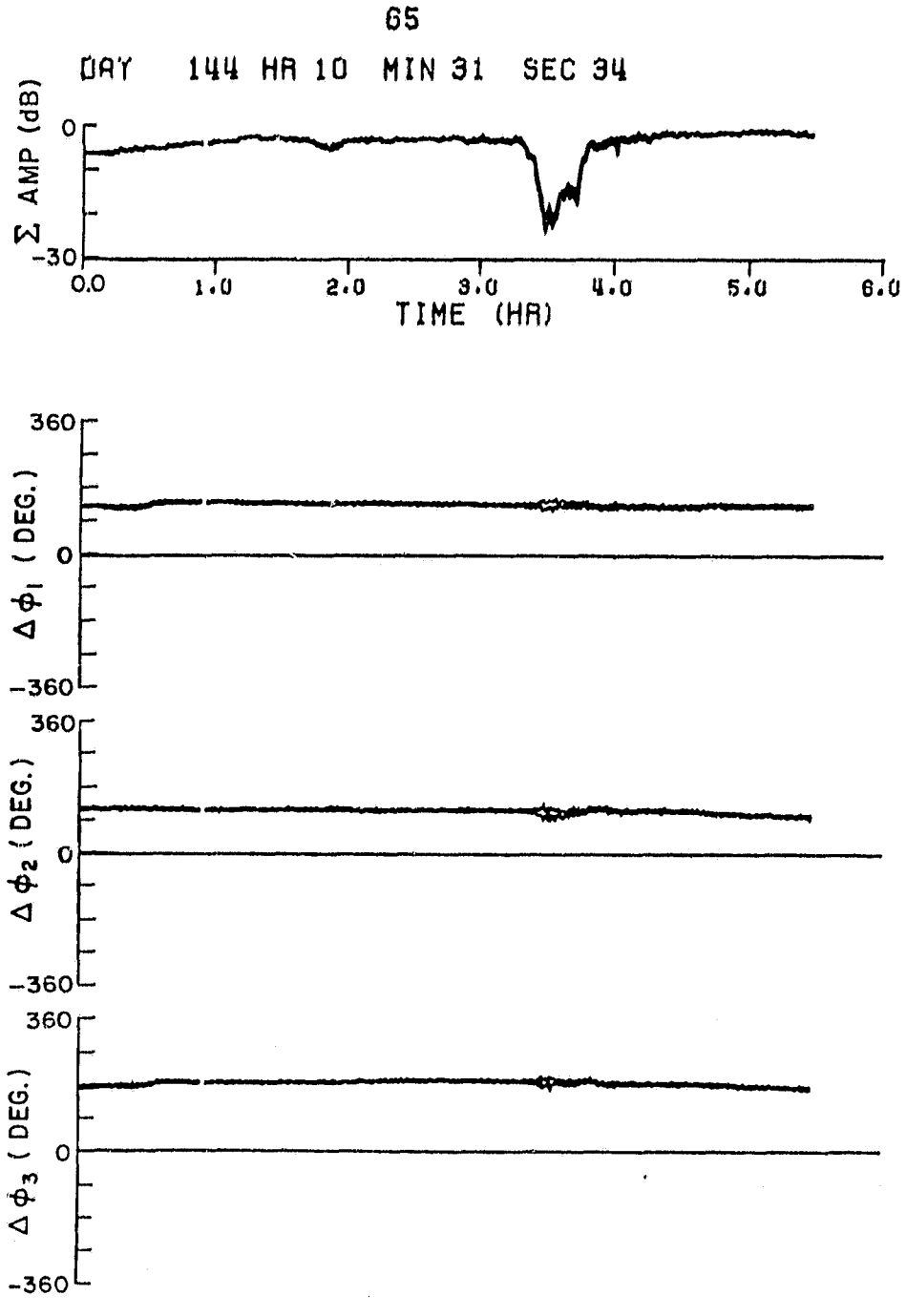

Figure 11. Received signals on day 144/1979. 1031Z

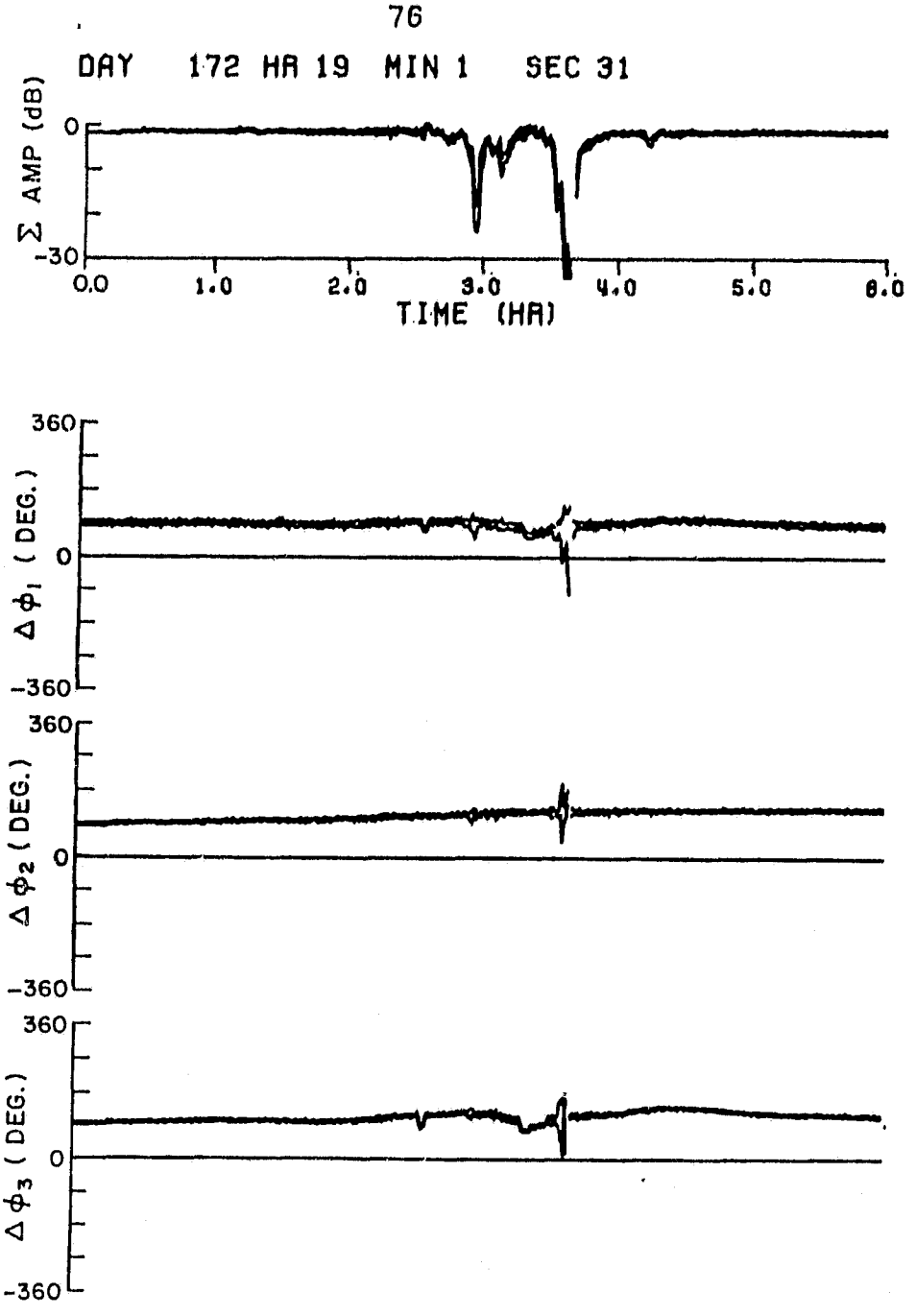

Figure 12. Received signals on day 172/1979. 1901Z

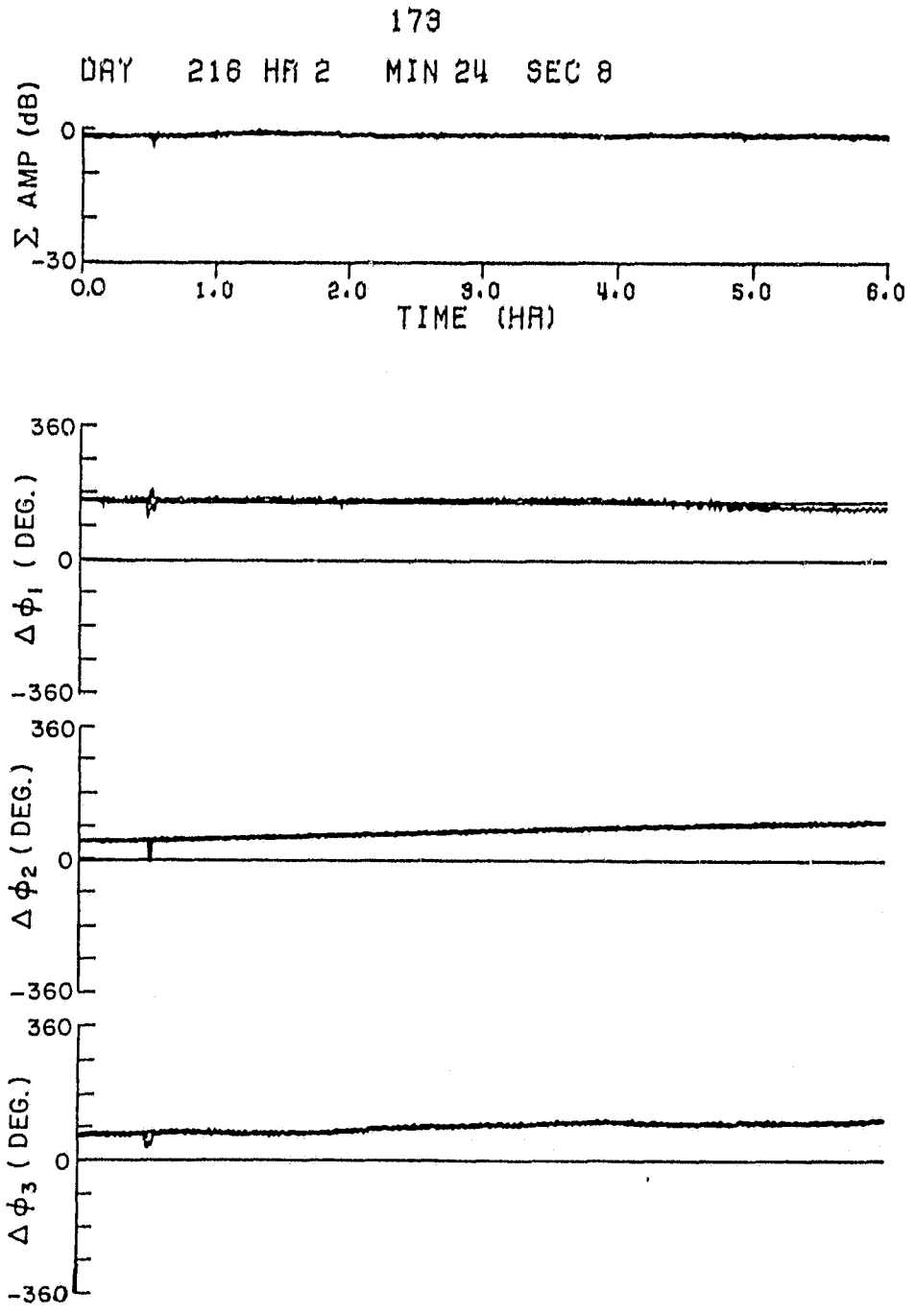

Figure 13. Received signals on day 216/1979. 0224Z

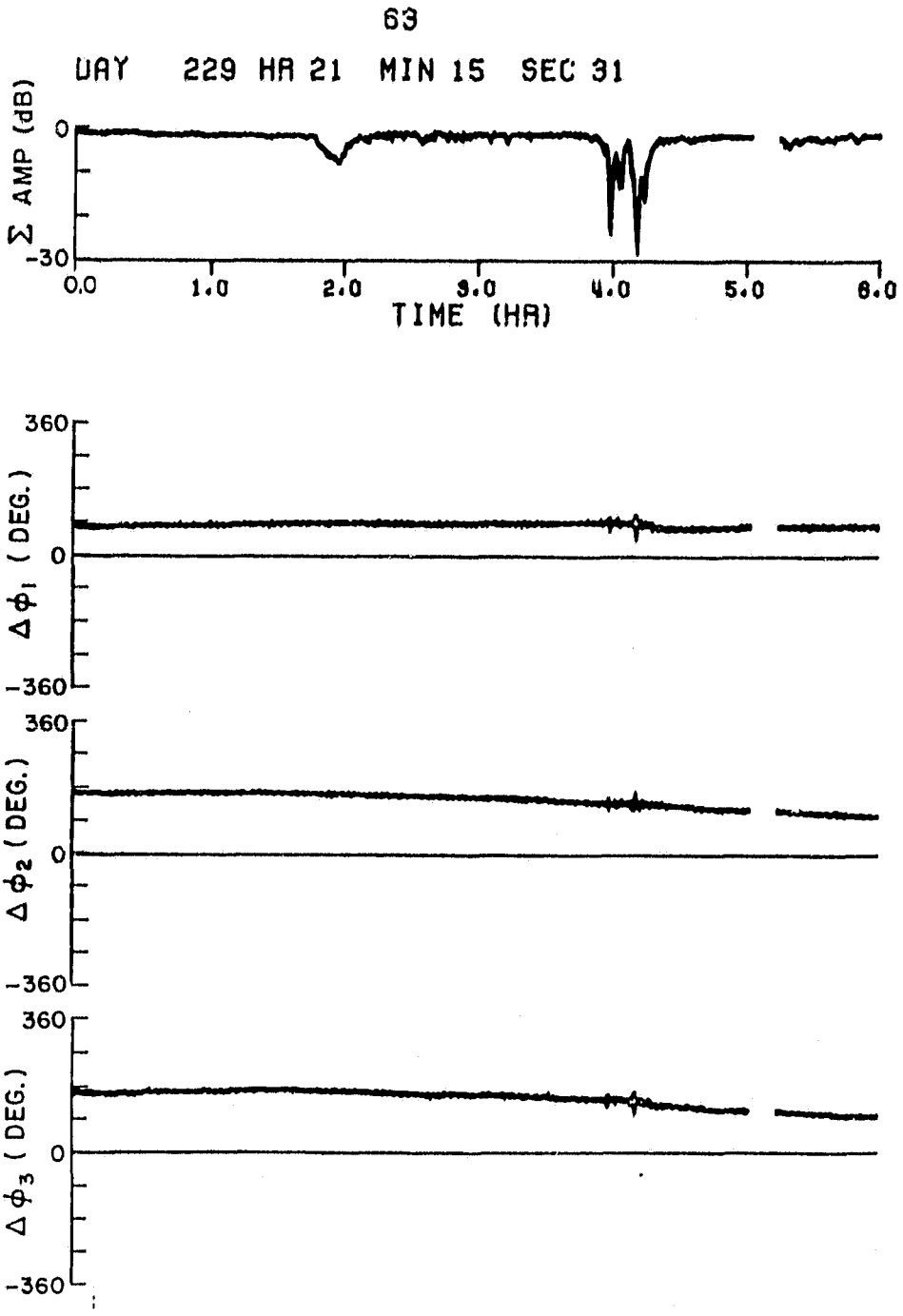

Figure 14. Received signals on day 229/1979. 2115Z

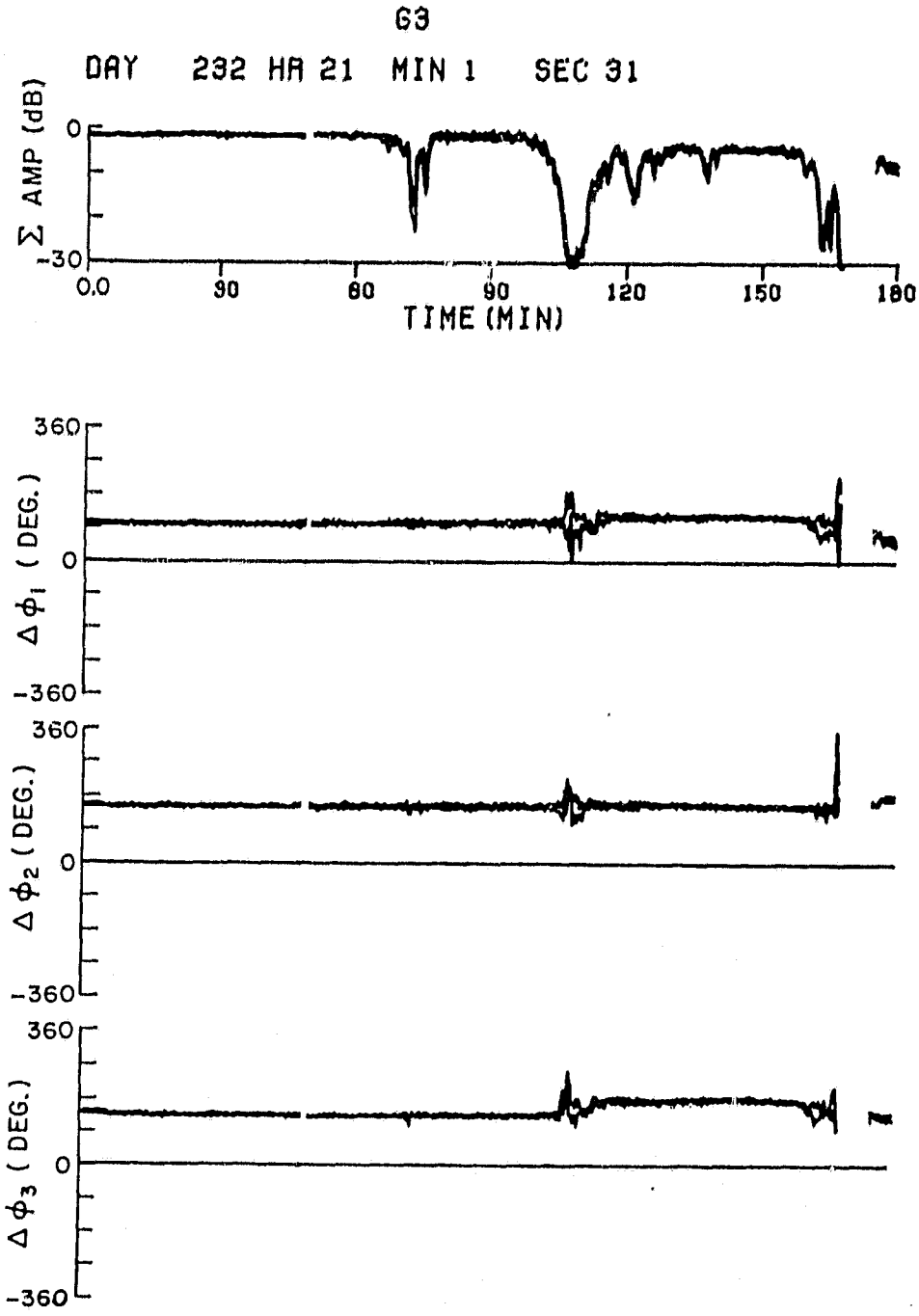

Figure 15. Received signals on day 232/1979. 2101Z

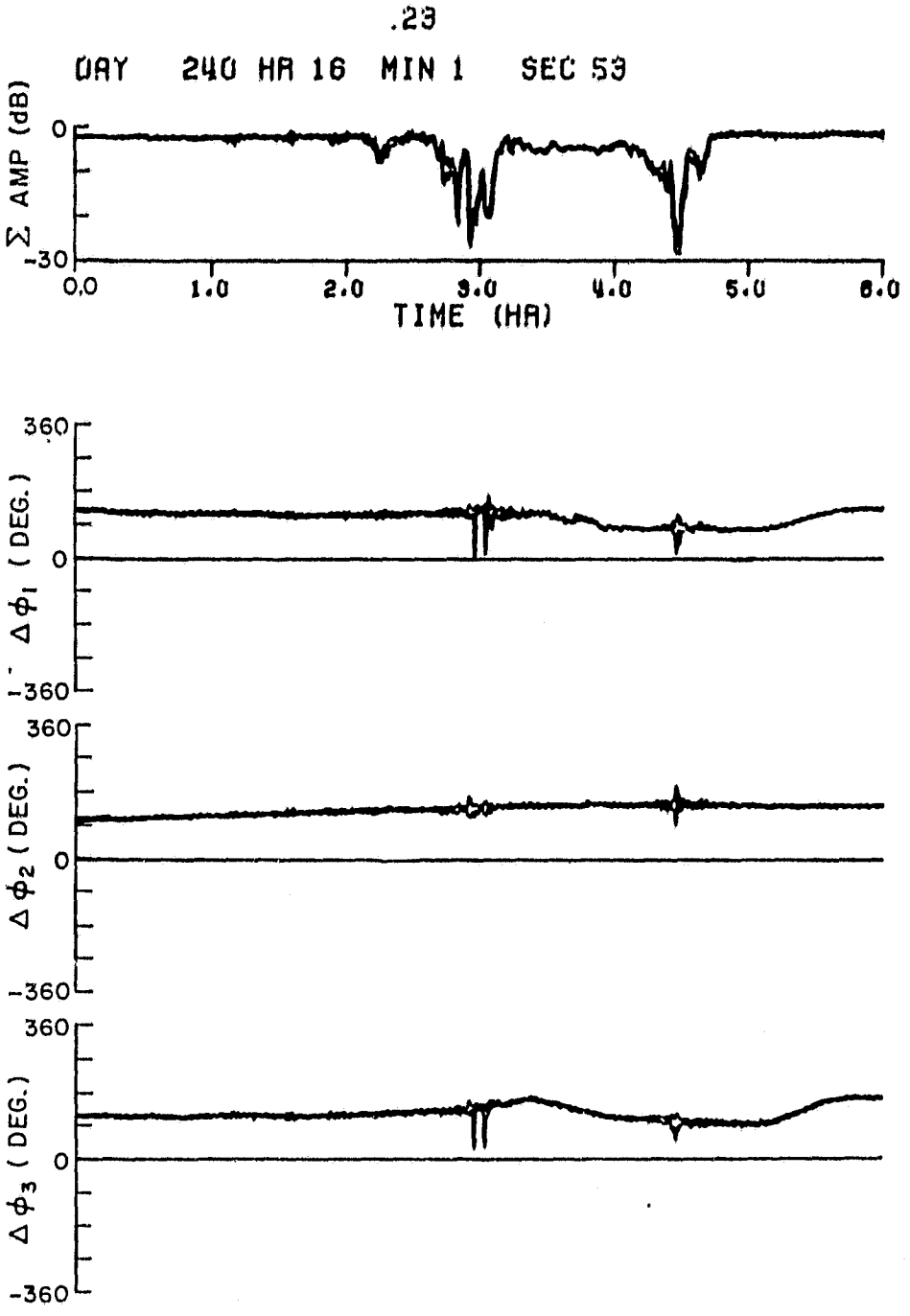

Figure 16. Received signal on day 240/1979. 1601Z

are subordinate at least down to that level. The data at the trough of the 29dB fade on day 232/79, 2250Z hours, Figure 15, on the other hand seems to show some effects of system noise in the fairly large excursions of all the differential phases.

The change in the mean levels of $\Delta\phi_1$ and $\Delta\phi_3$ after 2000Z hours in Figure 16, is believed to be due to drift in the receiver channel #1, which is common to these two differential phases.

Distributions

Figures 17 through 25 show monthly and quarterly distributions as well as the overall distributions for the period September, 1978, to September, 1979. The distributions of the amplitude, differential phase, and their variances are plotted.

The seasonal variation is seen clearly in Figures 17 through 25. Spring and summer rains cause the deepest fades and largest variance with the July result indicating that fades of 29dB were seen for about 0.001% of the time of observations (about 5 minutes per year). Winter months with the lower probability of rainfall show the least attenuation. The trend is seen more clearly in the quarterly distributions shown in Figures 18, 19, 21, 23-25.

Amplitude Variance

Quarterly amplitude variance distribution shown in Figure 19 show trends similar to the amplitude distributions. Smallest variances are observed in the first quarter. The tails of the distribution for the other three quarters, however, cross over, preventing general conclusions from being drawn. The lowest variance observed was almost 50dB below the DC power level of the received signal. This variance increased more than 30dB during rain events; this quantity must be tempered by the fact that the statistics during a fade event are not stationary and, hence, represent at best, an estimate.

Angle of Arrival

(a) Horizontal Channels Figures 20, 21, show azimuthal changes in angle of arrival which could be caused by horizontal variations in the refractive index of the atmosphere. The very low angle of arrival changes

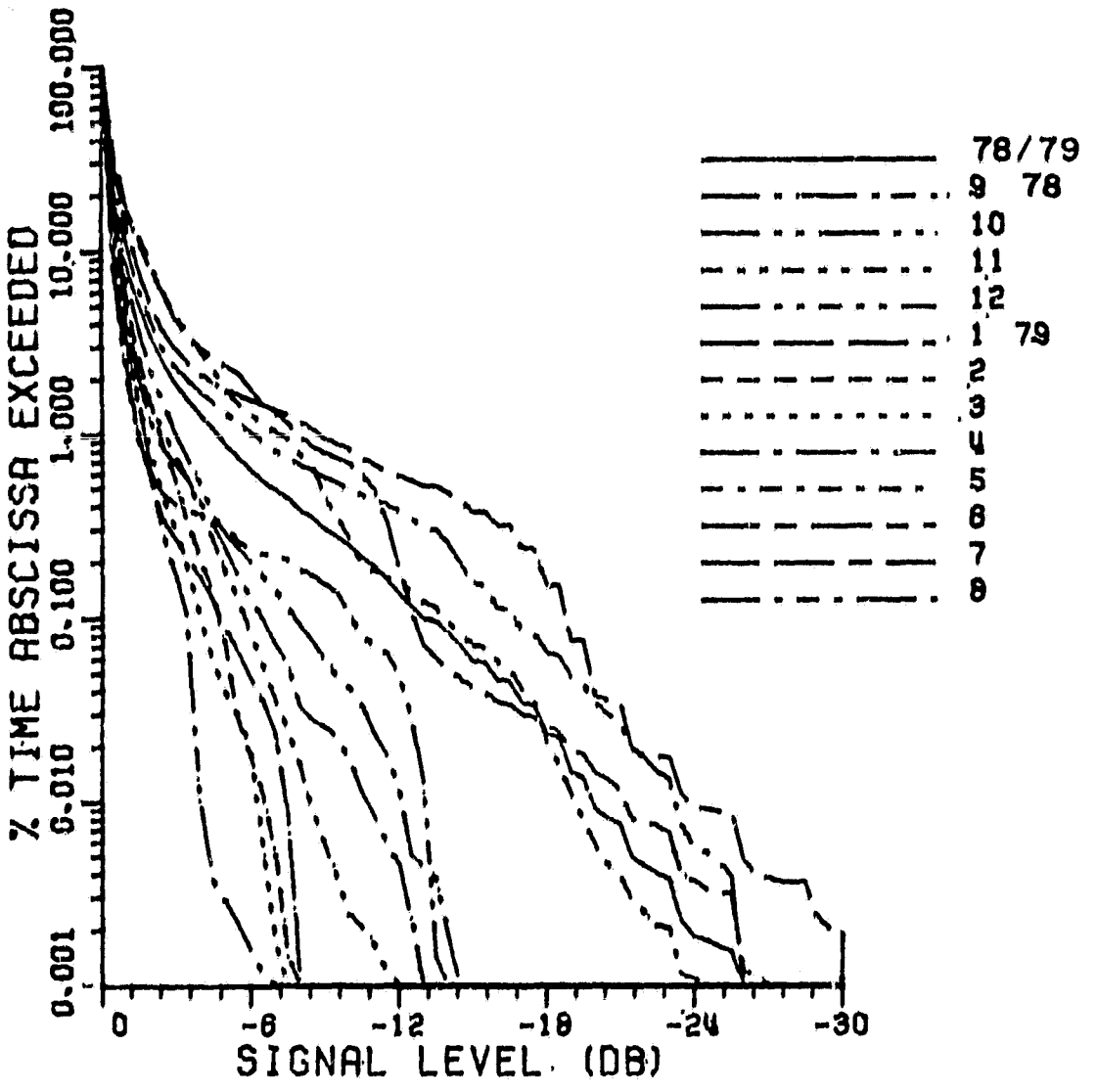

Figure 17. Monthly distribution of signal level.

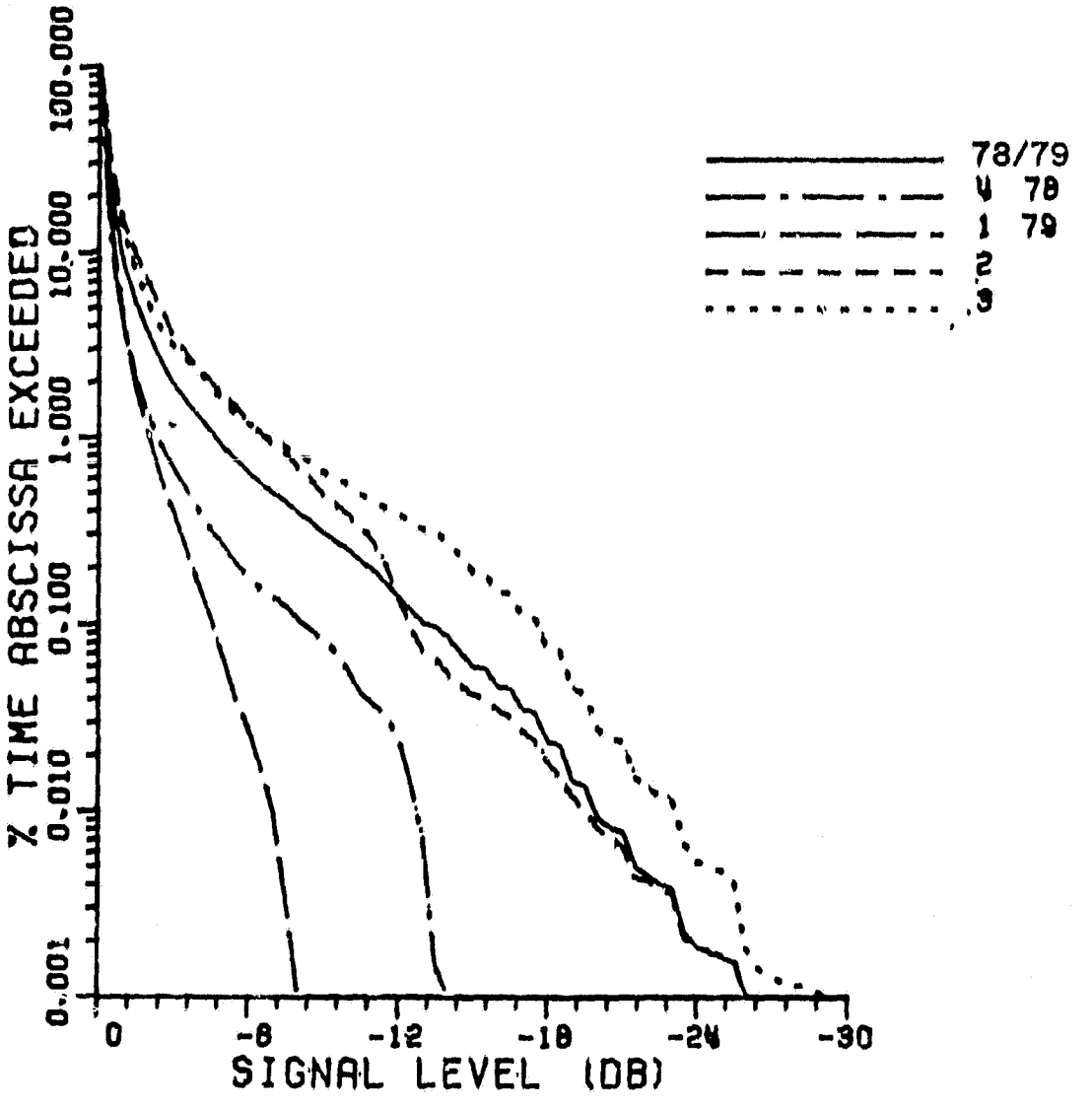

Figure 10. Quarterly distribution of signal level.

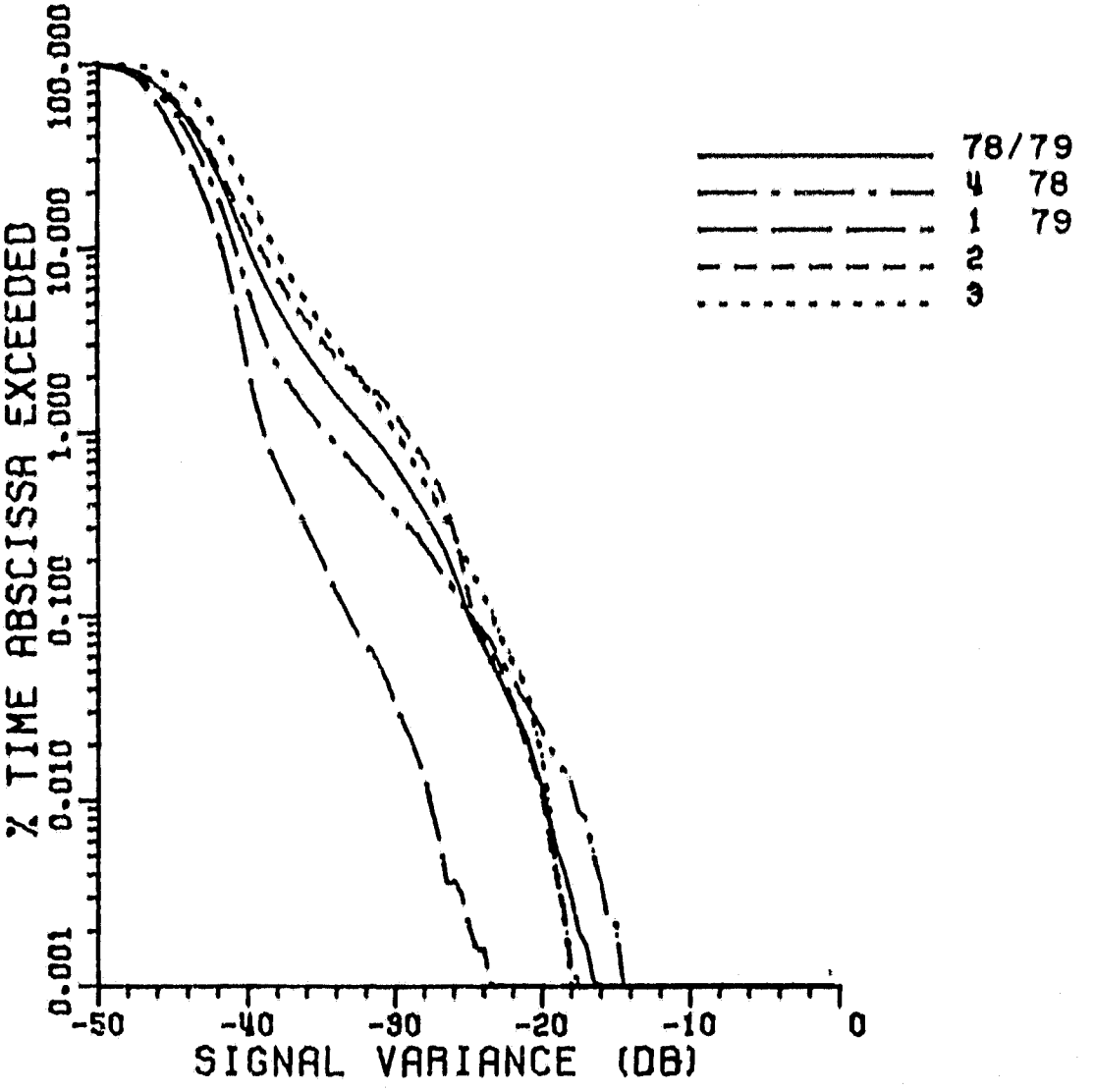

Figure 19. Quarterly distribution of signal level variance.

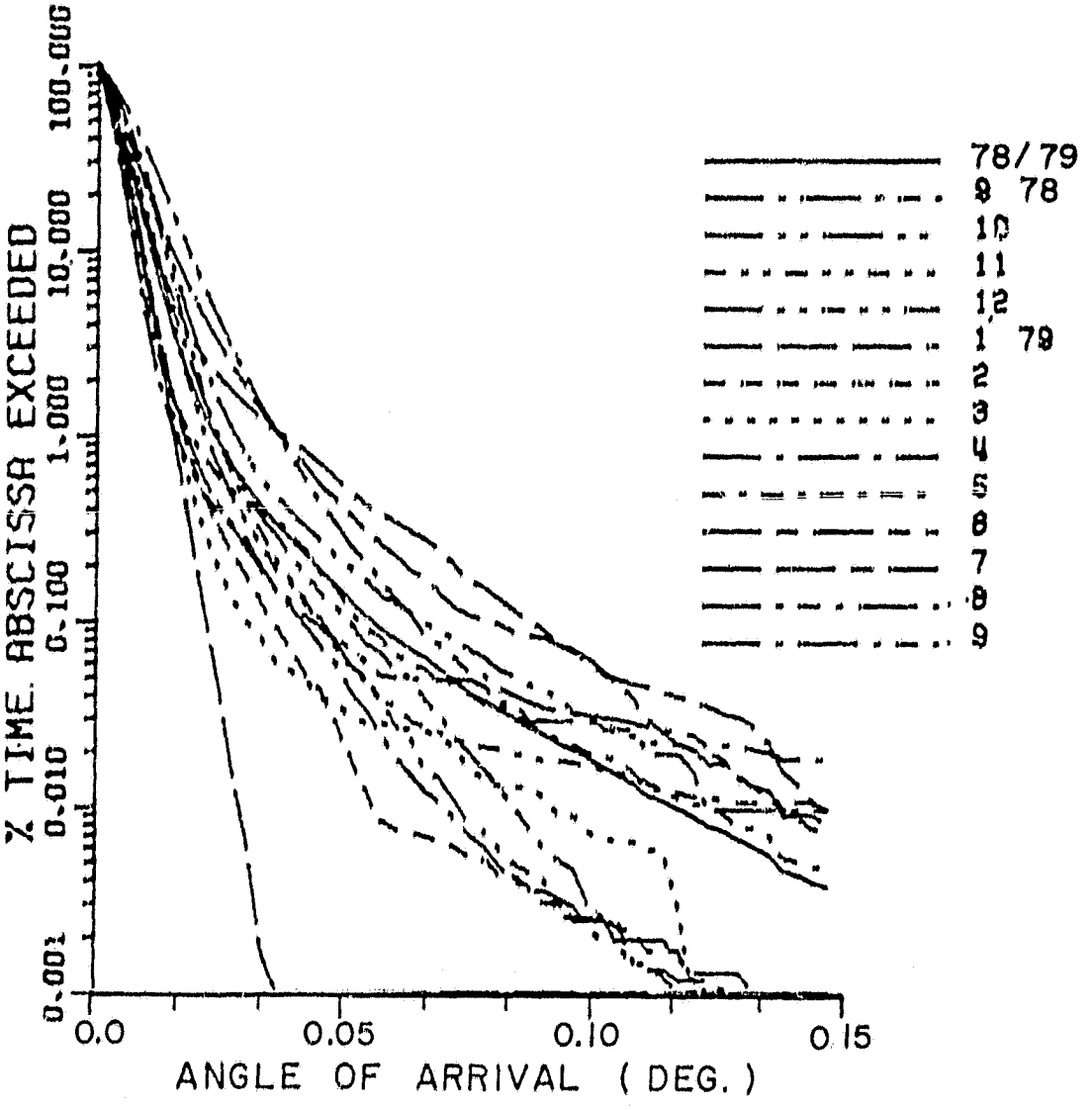

Figure 20. Monthly distribution of angle of arrival, azimuthal channel.

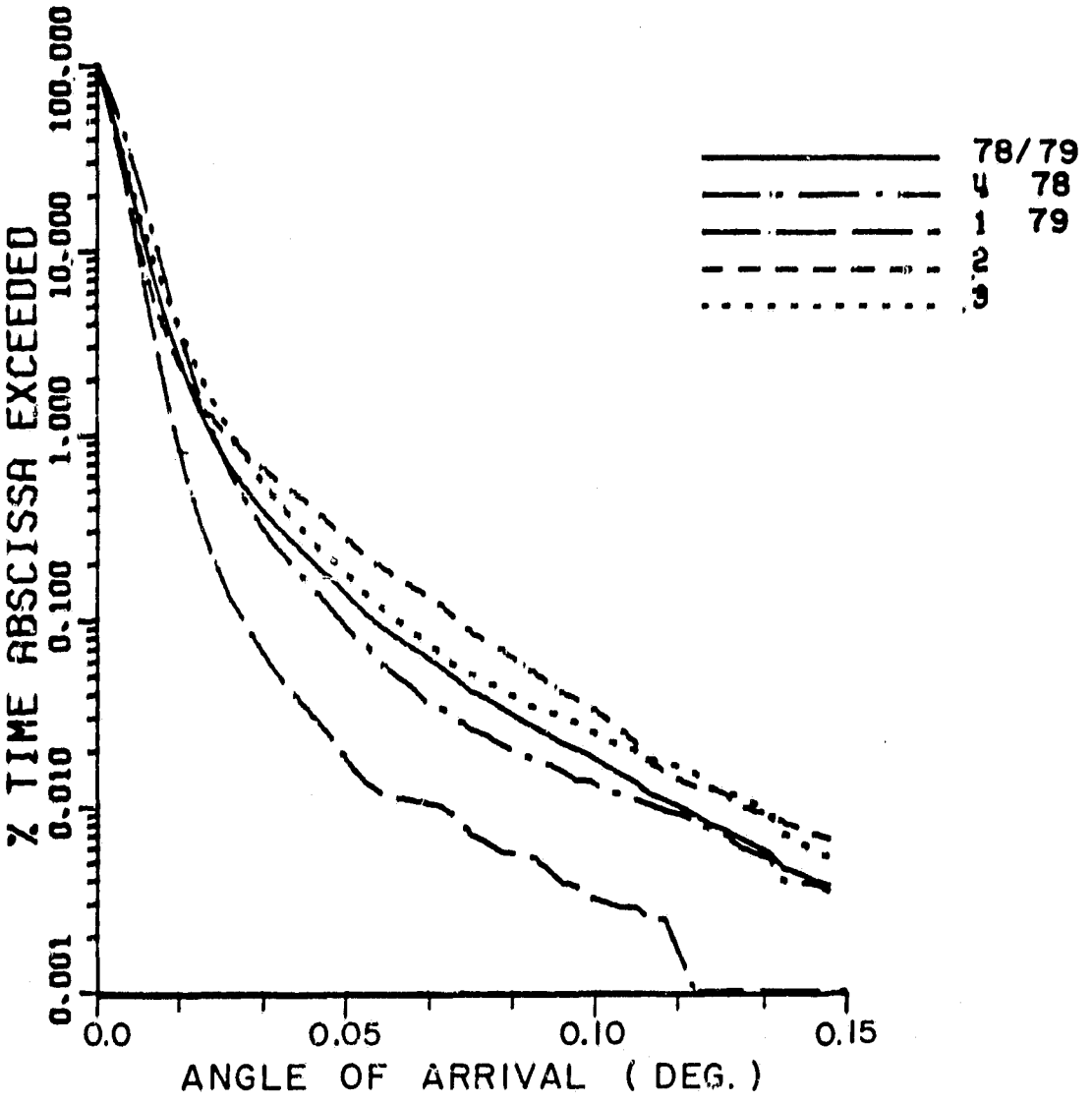

Figure 21. Quarterly distribution of angle of arrival, azimuthal channel.

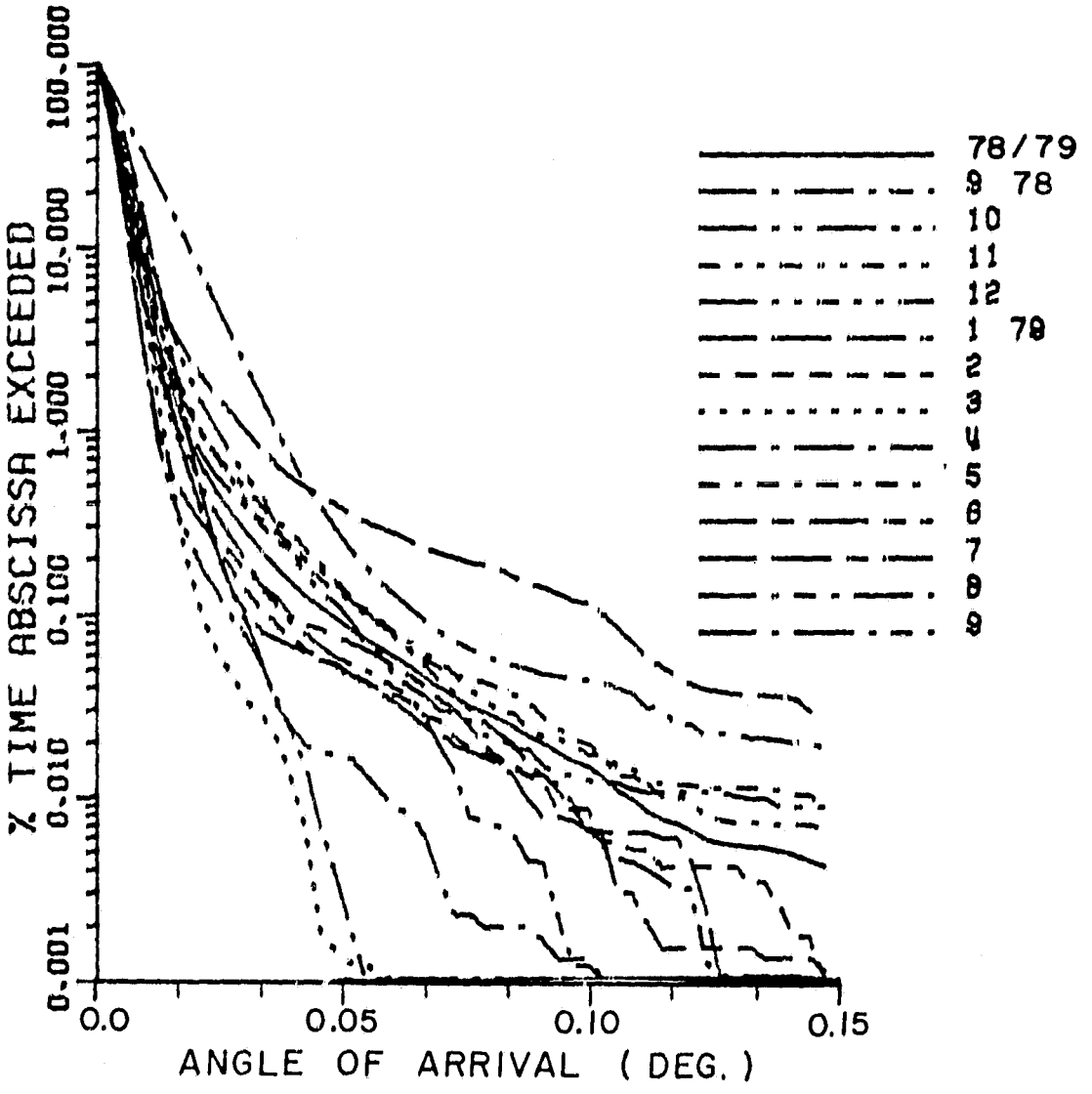

Figure 22. Monthly distribution of angle of arrival, elevational channel.

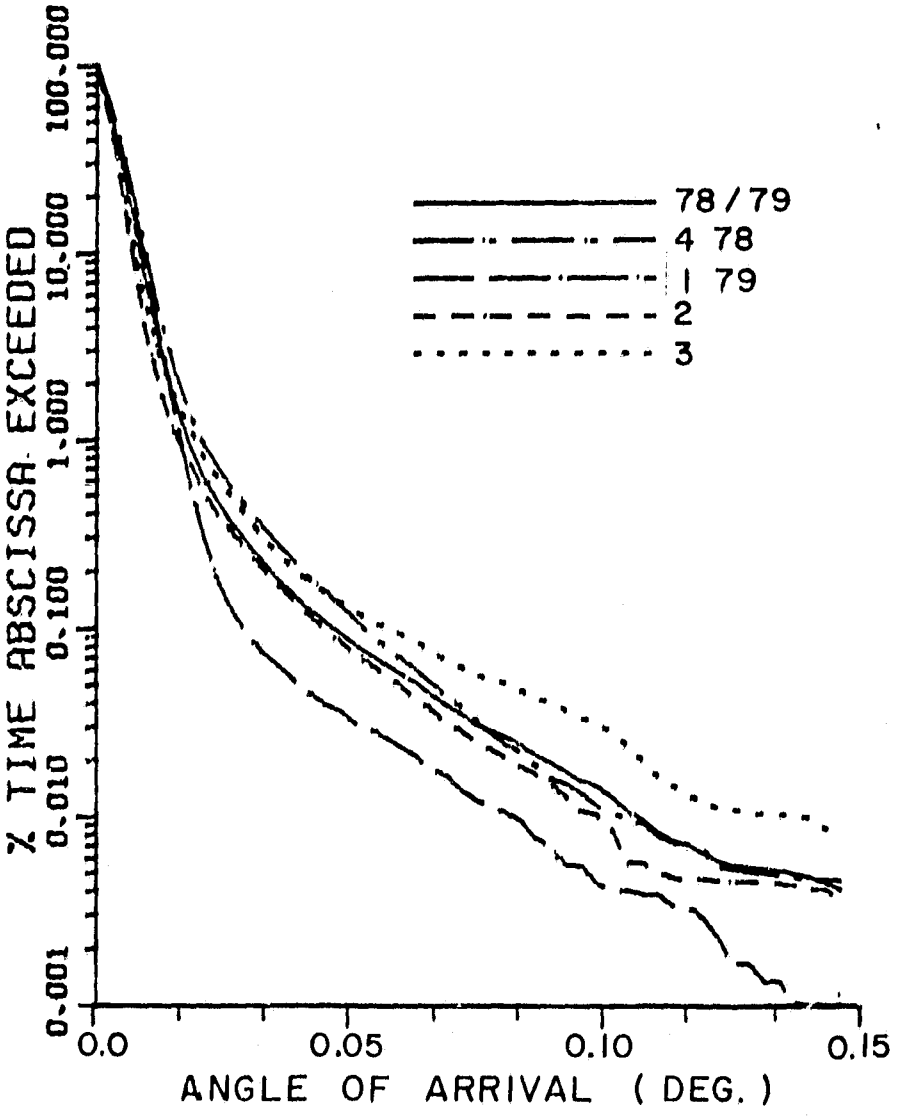

Figure 23. Quarterly distribution of angle of arrival, elevational channel.

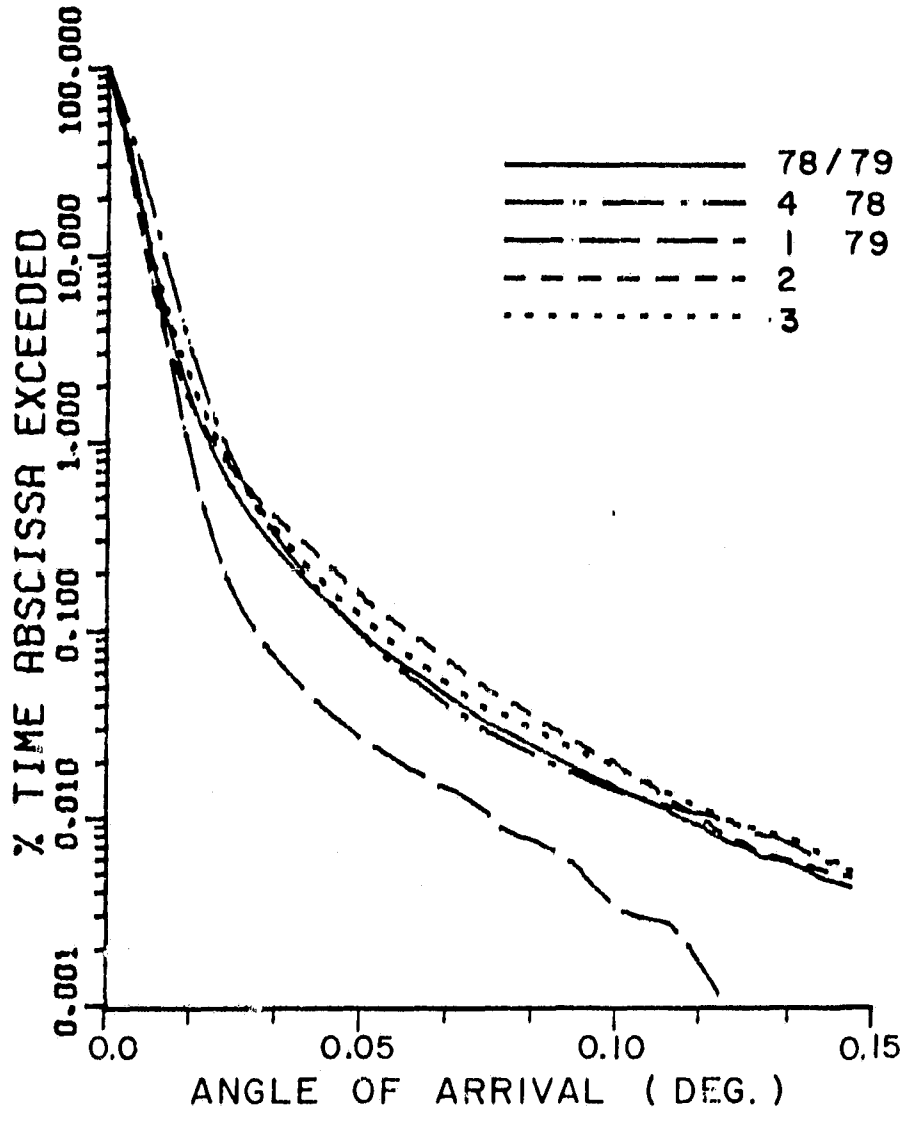

Figure 24. Quarterly distribution of angle of arrival; average of the azimuthal and elevational channels.

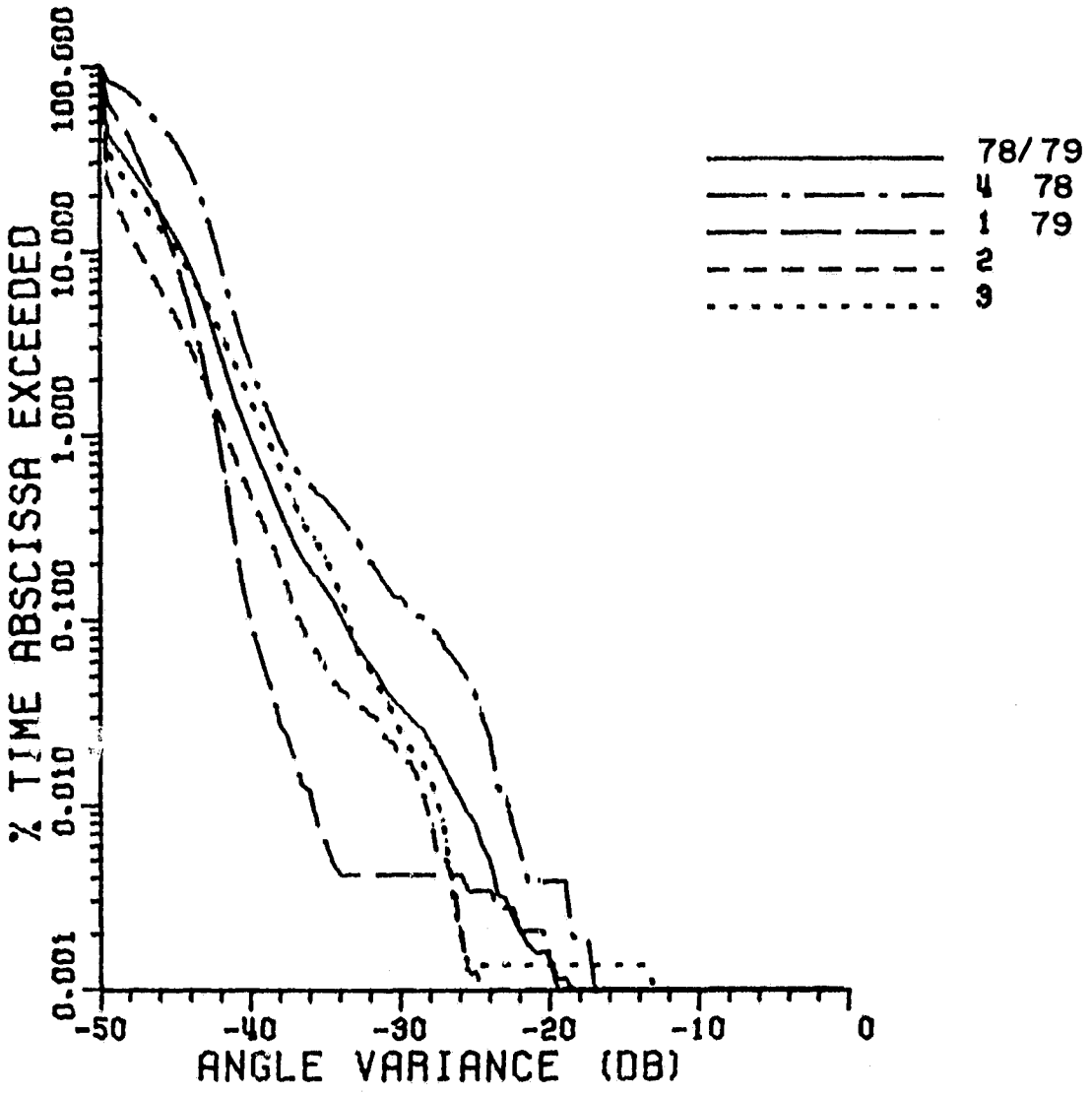

Figure 25. Quarterly distribution of angle of arrival variance; average of the azimuthal and elevational channels.

in January are striking. Angle of arrival fluctuations seem to peak in July. Most of these are perhaps the large fluctuations associated with rain fades. The second and third quarters of the year clearly show the largest angle of arrival fluctuations.

(b) Vertical Channels Figures 22, 23 show elevational changes in angle of arrival, which could be caused by variations in the refractive index in the vertical direction. Here, March displays the smallest angle changes with January being considerably higher. July, once more exhibits the largest angle fluctuations.

Angle of Arrival Variance

Quarterly distributions of angle variance averaged over all the channels are shown in Figure 25, together with the overall annual distribution. Once again, the smallest variance is seen in winter. The other quarters, however, do not follow the trend of the angle of arrival distributions.

The angle of arrival data were examined to see if any evidence of preferred anisotropy of the atmosphere was present. This would result in excursions of the wave about the horizontal axis being different from those about the vertical axis. The results were inconclusive, indicating that any anisotropy is weak at most, although it is interesting to note that the variability of the distributions of vertical angle changes is distinctly smaller than that associated with the horizontal angle changes.

Correlation

The correlation between differential phases is a measure of the degree to which the incoming wave approximates a plane wave. Hence, distributions of correlations were obtained for the third quarter of 1979, when all the differential phase channels were recorded. This is shown in Figure 26.

It is seen that the correlation coefficient distributions between the horizontal pairs as well as the verticals pairs are almost identical.

Further, it is intriguing that the median correlation coefficient

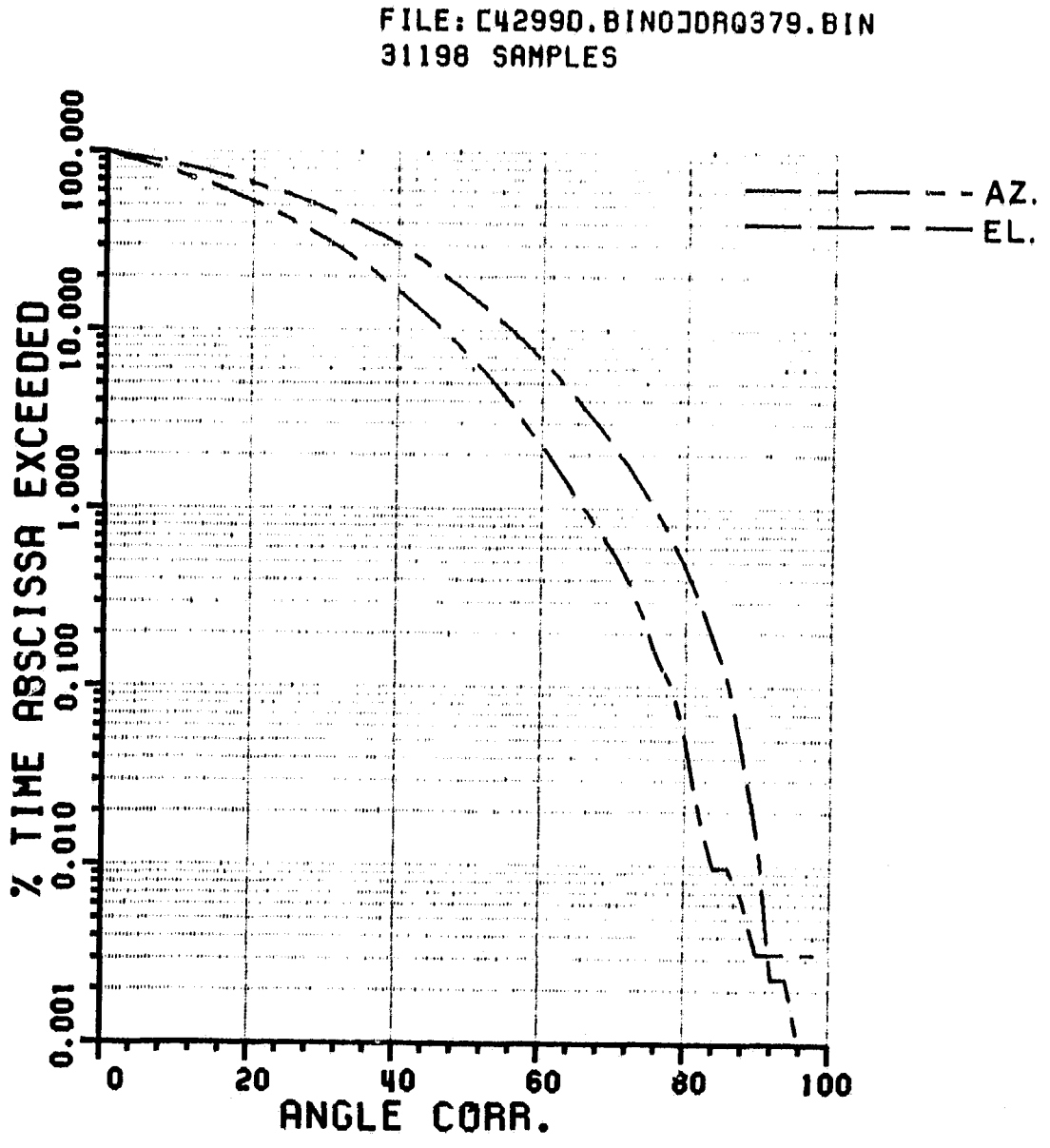

Figure 26. Distribution of angle of arrival correlation between the azimuthal differential phases and between the elevational differential phases.

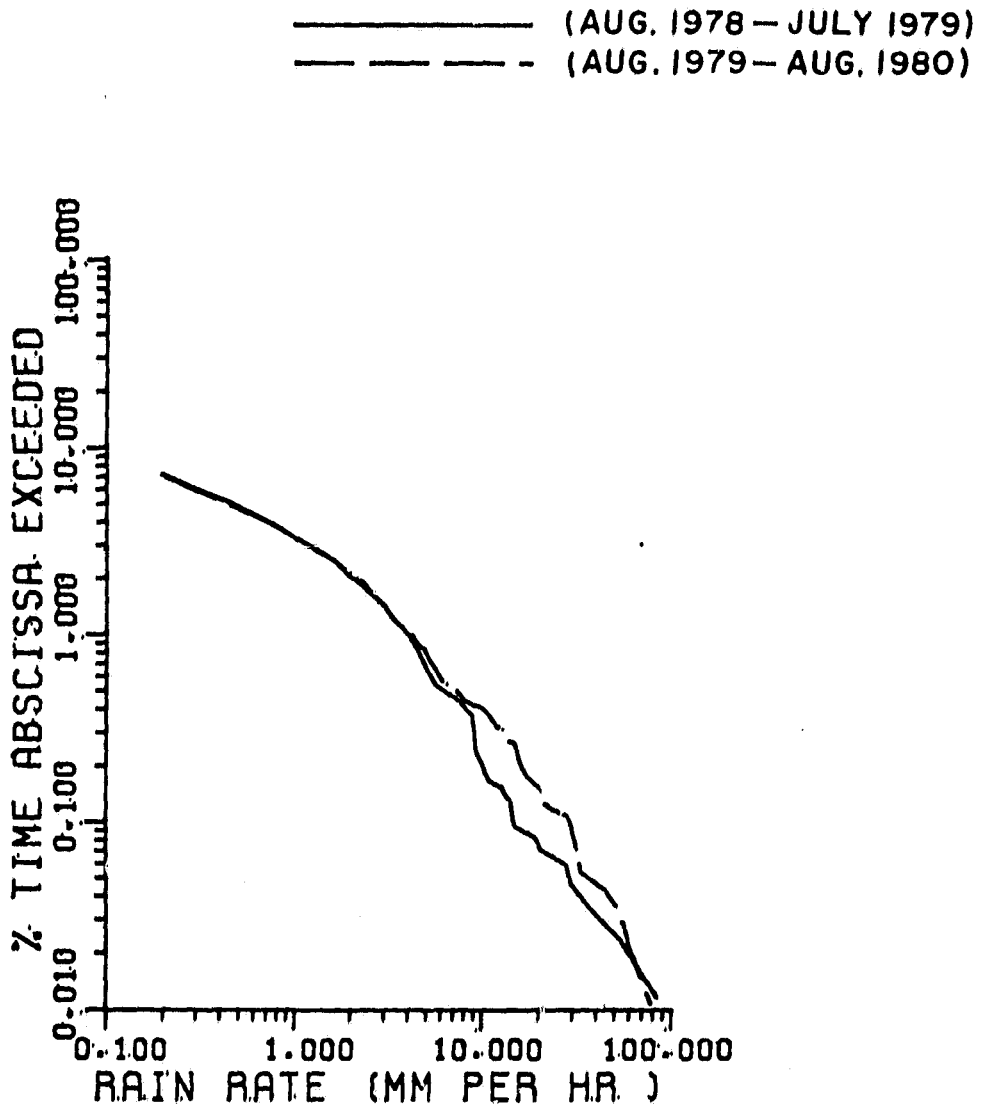

Figure 27. Rain rate distribution for the period August 1978 to August 1980.

remains quite small, at 20%. However, it rises to 82% for 0.01 per cent of the time. Of course, during clear sky conditions, the variance is small and probably largely due to front end noise. These noise contributions should, indeed, be uncorrelated. In contrast, during disturbed atmospheric conditions, the correlation should be higher, as is the case.

The rain rate distribution for the first 12 months of D_3 operation is shown in Figure 27. Also shown here is the corresponding distribution covering the next 13 months for comparison purposes.

In summary, one can note the following specific characteristics of the statistics presented in this section:

1. Amplitude Fluctuations
   Median value = less than 0.3 dB below maximum received amplitude,
   greater than 29 dB for .001% of time.
2. Amplitude Variance
   Median value = -42 dB below DC power level,
   greater than -16 dB for .001% of time.
3. Angle of Arrival (physical)
   Median fluctuation $.003^{o}$ peak, $.006^{o}$ peak-peak for .01% of time.
   greater than $.12^{o}$ peak, $.24^{o}$ peak-peak for .01% of time.
4. Angle variance
   Median value ≈ -50 dB,
   greater than -18 dB for .001% of time.

CONCLUSIONS

Amplitude and angle of arrival statistics are presented for a 28.56 GHz space-earth link using the CW beacon on the COMSTAR D_3 spacecraft. The data cover the period September 1978 to September 1979. Fades in excess of 29 dB were observed of 0.001% of the time of observation. Angle of arrival fluctuations exceeded 0.12 spatial degrees peak, or 0.24 degrees peak to peak for about 0.01% of the time. This fluctuation exceeds the beamwidth of a 5 meter antenna operating at 30 GHz. Thus, one would expect to see gain degradation in addition to amplitude attenuation under these conditions.

This experiment has continued and further results will be presented in a forthcoming report.

REFERENCES

[1] D.M. Theobold and D.B. Hodge, "The OSU Self-Phased Array for Propagation Measurements using the 11.7 GHz CTS Beacon", Report 4299-1, November 1976, The Ohio State University ElectroScience Laboratory, Department of Electrical Engineering; prepared under contract NAS5-22575 for National Aeronautics and Space Administration, Goddard Space Flight Center.

[2] D.M. Theobold and D.B. Hodge, "ATS-6 Millimeter Wavelength Propagation Experiment", Report 3863-4, April 1975, The Ohio State University ElectroScience Laboratory, Department of Electrical Engineering; prepared under contract NAS5-21983 for National Aeronatuics and Space Administration, Goddard Space Flight Center.

[3] B.W. Kwan and D.B. Hodge, "The CTS 11.7 GHz Angle of Arrival Experiment", Report 712759-2, January 1981, The Ohio State University ElectroScience Laboratory, Department of Electrical Engineering; prepared under contract NASW-3393 for National Aeronautics and Space Administration, Headquarters.

ACKNOWLEDGMENTS

The basic conversion of the receiving system to the COMSTAR satellite was performed by messers R.C. Taylor and D.M. Henry.

The contributions of R.A. Baxter during the early periods of the experiment and in the initial stages of software development is also gratefully acknowledged.